Oncology: Neuroblastoma

13

Maria Felicia Villani, Milena Pizzoferro, Aurora Castellano, Roberta Lombardi, Annalisa Serra, Maria Carmen Garganese, and Franco Locatelli

13.1 Introduction

Neuroblastoma is the most common solid extracranial tumor of childhood. It originates from the cell of the neural crest intended to form sympathetic nervous system. It accounts for 7 % of all childhood cancers and for approximately 15 % of cancer deaths in children. Most frequently neuroblastoma arises from the adrenal gland (65 %) but it could originate along the ganglia of sympathetic nervous system. Other common sites are the ganglia in the retroperitoneum followed by the ganglia localized in the chest, neck, and pelvis. The median age at diagnosis is 17 months, but it can occur in children from the prenatal age to young adult age. Around 50 % of patients present with disseminated disease at the time of diagnosis. Dissemination occurs through lymphatic and hematogenous routes, with the involvement of bone, bone marrow, and liver.

Neuroblastoma is staged according to the International Neuroblastoma Staging System (INSS). Stage 1 or 2 neuroblastoma is localized, stage 3 neuroblastoma consists of locoregional extended disease, and stage 4 neuroblastoma is marked by distant metastases. A unique pattern of dissemination, limited to the liver, skin, and less than 10 % of bone marrow in children younger than 18 months old, is defined as stage 4S, which has a potential for spontaneous regression.

M.F. Villani • M. Pizzoferro
Nuclear Medicine Unit, Imaging Departement – "Bambino Gesù" Children Hospital, Rome, Italy

A. Castellano (✉) • A. Serra • F. Locatelli
Oncohematology Department, "Bambino Gesù" Children Hospital, Rome, Italy
e-mail: aurora.castellano@opbg.net

R. Lombardi
Imaging Department, "Bambino Gesù" Children Hospital, Rome, Italy

M.C. Garganese
Diagnostic Imaging Department of Nuclear Medicine, IRCCS Bambino Gesù Paediatric Hospital, Rome, Italy

During the last two decades, there have been major advances in understanding the genetics of NB. Although the unfavorable prognostic factor MYCN amplification is used by all cooperative groups for risk-group stratification and therapeutic decisions, other prognostically significant genetic features have been incorporated into risk classification schemas. For these reasons, the International Neuroblastoma Risk Group (INRG) published a new clinical staging system in 2008: the INRG classification was designed to stratify patients at the time of diagnosis; before any treatment, in the International Neuroblastoma Risk Group Staging System (INRGSS), extent of locoregional disease is determined by the absence or presence of image-defined risk factors (IDRFs) (L1 and L2, respectively). Stage M will be used for widely disseminated disease, and MS describes metastatic NB limited to skin, liver, and bone marrow, without cortical bone involvement in children aged 0–18 months with L1 or L2 primary tumors. This new stratification takes into account histology, age, stage at diagnosis, and chromosomal aberrations.

Children with metastatic disease are quite ill at presentation. As the tumor disseminates to the bone, patients often present with nonspecific symptoms such as fever, bone pain, limping, or all of these. Metastasis in the orbits can cause periorbital ecchymosis (raccoon eyes), sometimes accompanied by proptosis, caused by metastases in the orbital bone.

Particular clinical presentation of disease are the tumor arising from paraspinal site that may cause spinal cord compression resulting in neurological symptoms, such as motor weakness, pain, and sensory loss, which can be medical emergencies. In these cases, multidisciplinary competences are required.

Clinical presentation of patients affected by localized disease depends on the site of tumor; so, the abdominal localization presented with abdominal pain, while thoracic localization often presented with cough or as an incidental finding.

The treatment of metastatic neuroblastoma generally consists of induction chemotherapy, surgery, myeloablative

M.C. Garganese, G.F.L. D'Errico (eds.), *Conventional Nuclear Medicine in Pediatrics*, DOI 10.1007/978-3-319-43181-9_13

chemotherapy with stem cell rescue, radiotherapy, and immunotherapy. The treatment of localized neuroblastoma ranges from observation to chemotherapy, surgery, radiotherapy, and differentiating therapy. The clinical course in patients affected by metastatic neuroblastoma varies enormously, ranging from spontaneous regression to rapid and fatal tumor progression, despite extensive treatment.

The outcome of the patient affected by neuroblastoma is extremely variable in the case series and strongly depends on the presence of metastatic disease.

Improvement in the knowledge about tumor genome, more refined pathological definition, and more sophisticated diagnostic techniques allow to better characterize neuroblastoma in all its features, in order to tailor the treatment to the patients and to improve their prognosis.

13.2 Study Technique and Interpretation: 123I-MIBG Scintigraphy

123I-MIBG is administered by slow intravenous injection (administered activity adjusted to the patient's weight, according to EANM dosage card and to the Italian regulations), and scintigraphic images are acquired 24 h after the injection.

Anterior and posterior static spot images of chest, abdomen, pelvis, upper and lower extremities, and anterior, posterior, left lateral, and right lateral spot images of the skull are acquired; the study is single proton emission tomography (SPECT) of interested segments; SPECT images are also manually fused with CT and/or MRI when available.

123I MIBG scan represents the gold standard for disease staging and treatment response evaluation in NB patients. MIBG labeled with 123I has superior imaging characteristics than 131I-MIBG due to its physical properties (159 keV photon energy, 13 h half-life, and paucity of 123I particulate emission) and to the high activity that can be administered. 123I characteristics and its favorable dosimetry, even at high administered doses, make its use preferable in children. Moreover, the SPECT and SPECT/CT overcome the limitation of planar 123I MIBG scan imaging and can distinguish false-positive uptake, thus improving the detection rate and accuracy. A better anatomical localization of the lesions is achieved by the three-dimensional reconstruction of CT images, while imaging definition is improved by the lesion contrast evident at the CT scan.

Overall, MIBG scintigraphy alone is a sensitive (88–93%) and specific (83–92%) tool in detecting NB cells. False-positive MIBG findings are due to misinterpretation of physiological uptake, as in normal adrenal gland, bowel, muscle, heart, and liver. Instead, MIBG uptake in bone or bone marrow is always abnormal and has to be considered as a sign of focal bone involvement and/or diffuse bone marrow infiltration.

There are many drugs that can interfere with MIBG uptake, in particular, cardiovascular and sympathomimetic drugs (such as amiodarone, combined alpha and beta-blockers, adrenergic neurone blockers, alpha-blockers, calcium channel blockers), systemic and local nasal decongestants, and several neurological drugs. A full list of interfering drugs is reported in EANM Guidelines on MIBG Scintigraphy.

However, in pediatric clinical practice, most used medications are cardiovascular drugs, in particular, antihypertensives, because hypertension is often present in NB patients.

13.2.1 Case 13.1 MIBG Scan in Prenatal Diagnosis of Adrenal Mass: MIBG-Avid Lesion

A newborn with prenatal diagnosis of right adrenal mass, confirmed by ultrasonography (US, 1) at birth and with elevated urinary catecholamines, undergoes 123I-MIBG scintigraphy (Fig. 13.1c, d) to confirm the suspicion of neuroblastoma (NB). MIBG scan shows a MIBG avid lesion, without evidence of metastases. According to European guidelines, the baby is enrolled in observational protocol for neonatal adrenal mass.

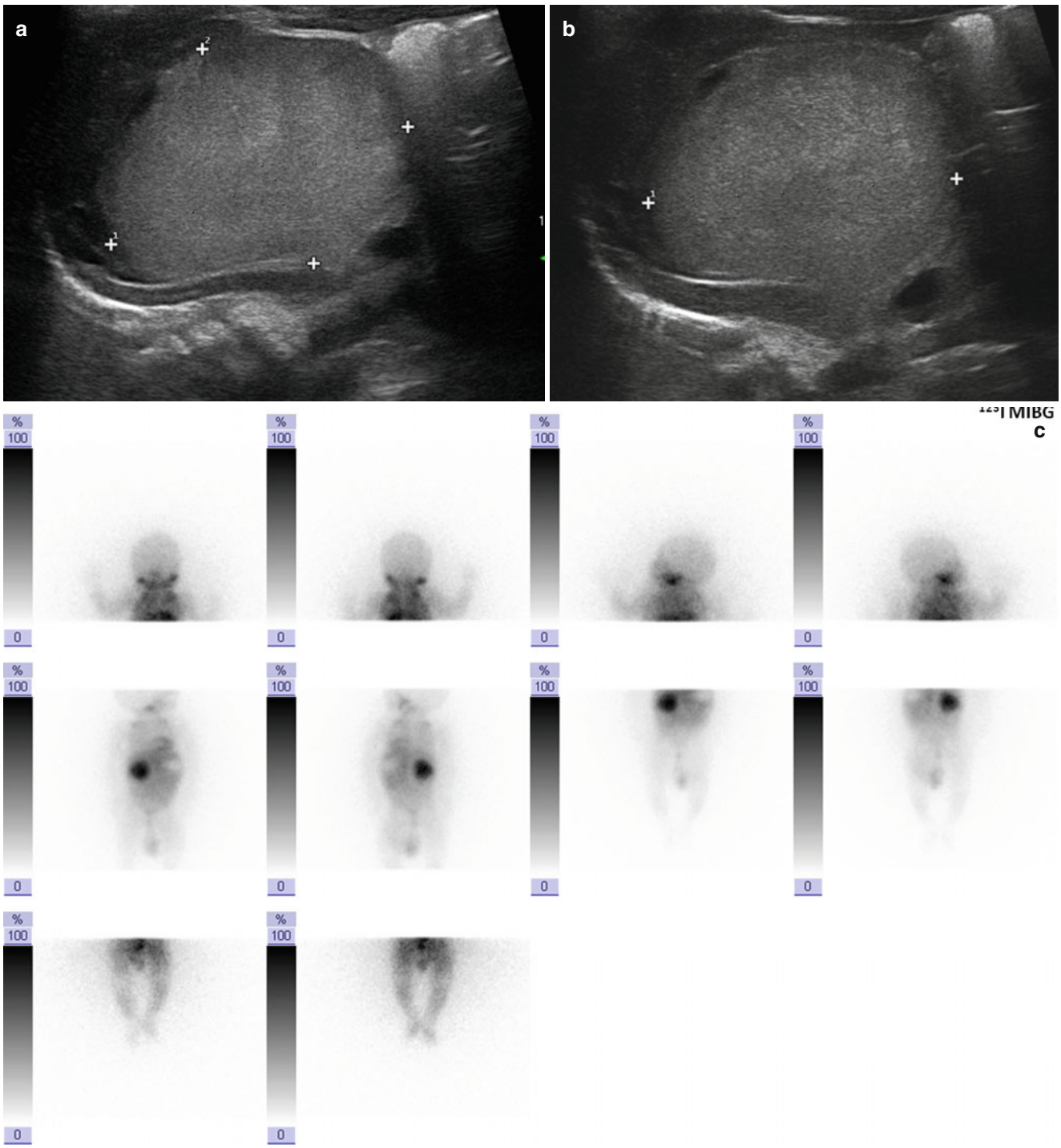

Fig. 13.1 (**a**, **b**) Ultrasonographic images detect a large, oval, "comma"-shaped suprarenal mass showing an echoic fine nonhomogeneous pattern; neither calcifications nor necrotic areas are seen within the lesion. Diameters are about 40 × 27.5 × 34.5 mm. Right kidney is displaced and distorted, but not infiltrated by the tumor, and adrenal flaps are opened wide; a "contact" is present between the mass and the inferior vena cava that appears "flattened," reduced in diameter in retrohepatic tract, but with partially visible lumen. Color-Doppler ultrasound (CDUS) evaluation shows some flow signal peripherally and within the lesion. (**c**, **d**) MIBG scintigraphy (static views (**c**) show an area of intense and nonhomogeneous radiotracer uptake in the abdomen, corresponding to the mass detected by ultrasonography; no other areas of pathological uptake of radiotracer are evident. SPECT images (**d**) help to better identify the site of the uptake (right adrenal region)

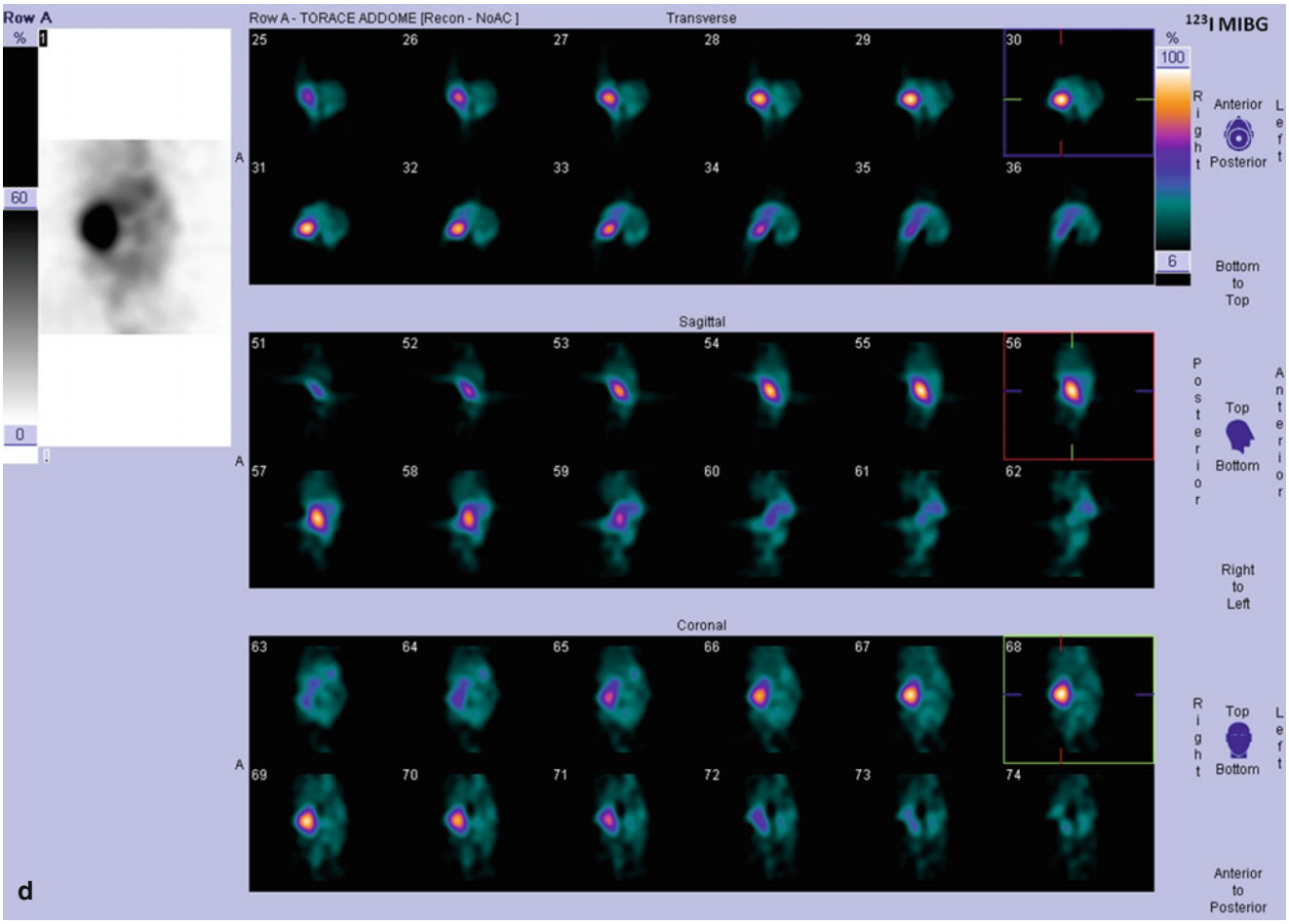

Fig. 13.1 (continued)

13.2.2 Case 13.2 Prenatal Diagnosis of Adrenal Mass: Nonavid Lesion at MIBG Scan

A newborn with prenatal diagnosis of left adrenal mass undergoes at birth an ultrasonography (Fig. 13.2a–d), which shows a reduction of diameters of the lesion; therefore, 123I-MIBG scintigraphy is performed in order to exclude a NB (Fig. 13.2e, f). The lesion appears as nonavid of MIBG, and the baby is enrolled in observational protocol for neonatal adrenal mass.

Lesion was no longer detectable at ultrasonography performed at 1 year of age.

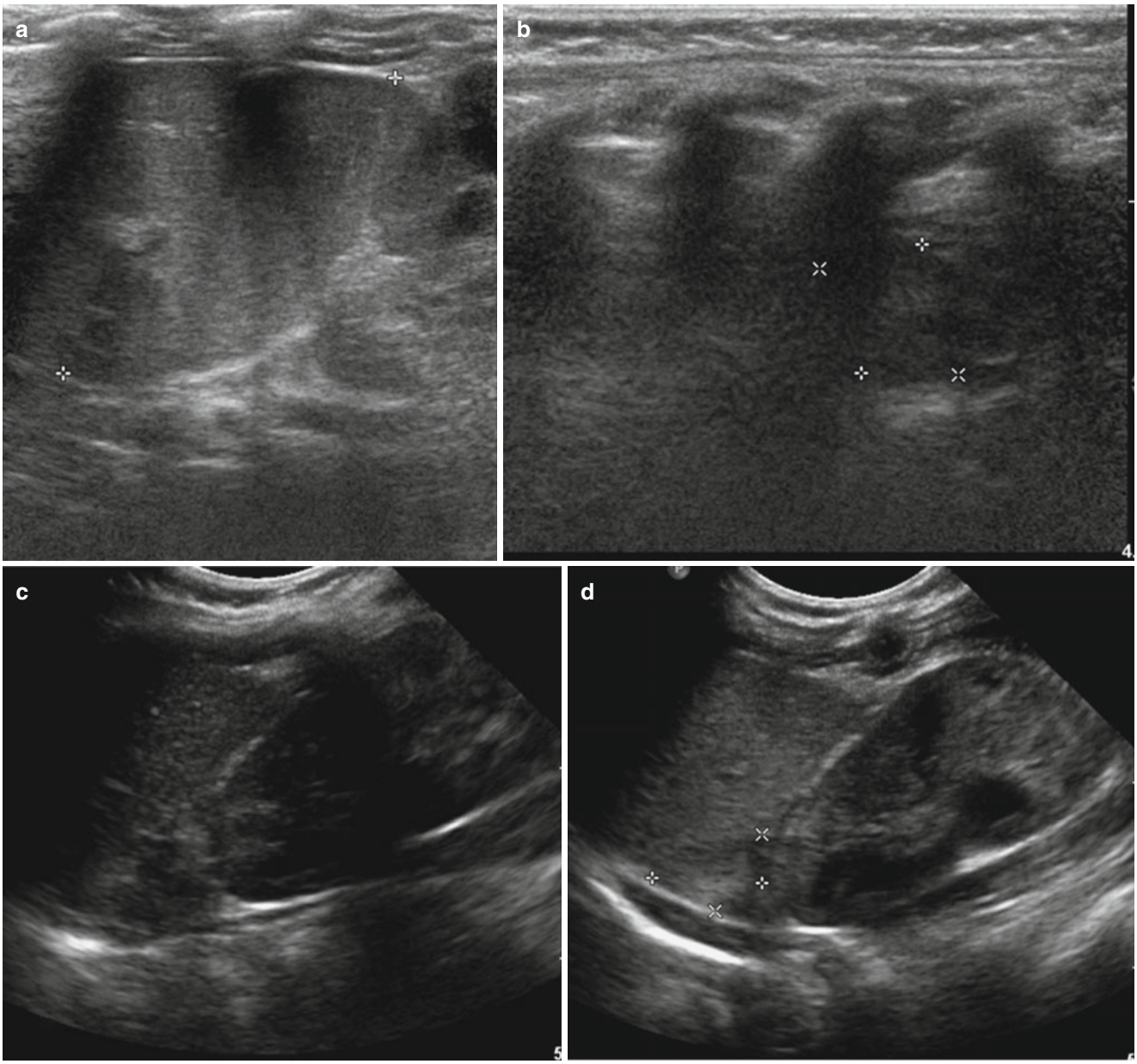

Fig. 13.2 (**a**–**d**) Ultrasonographic images of the left hypochondrium shows a lesion with size reduced compared to the previous ultrasound examination performed in gestational age (now measuring about 14 × 12 × 10 mm). This lesion presents another homogeneous pattern, mainly hypoechoic with tiny hyperechoic spots in the central part, probably due to small calcifications. At CDUS, no flow signals are detected within the adrenal mass. Spleen and left kidney are separated from the lesion by a fatty layer. (**e**, **f**) MIBG scintigraphy (static views, **c**) does not show any areas of pathological uptake of radiotracer; in particular, the lesion detected by ultrasonography appears as nonavid of MIBG. SPECT images (**f**) confirm this finding

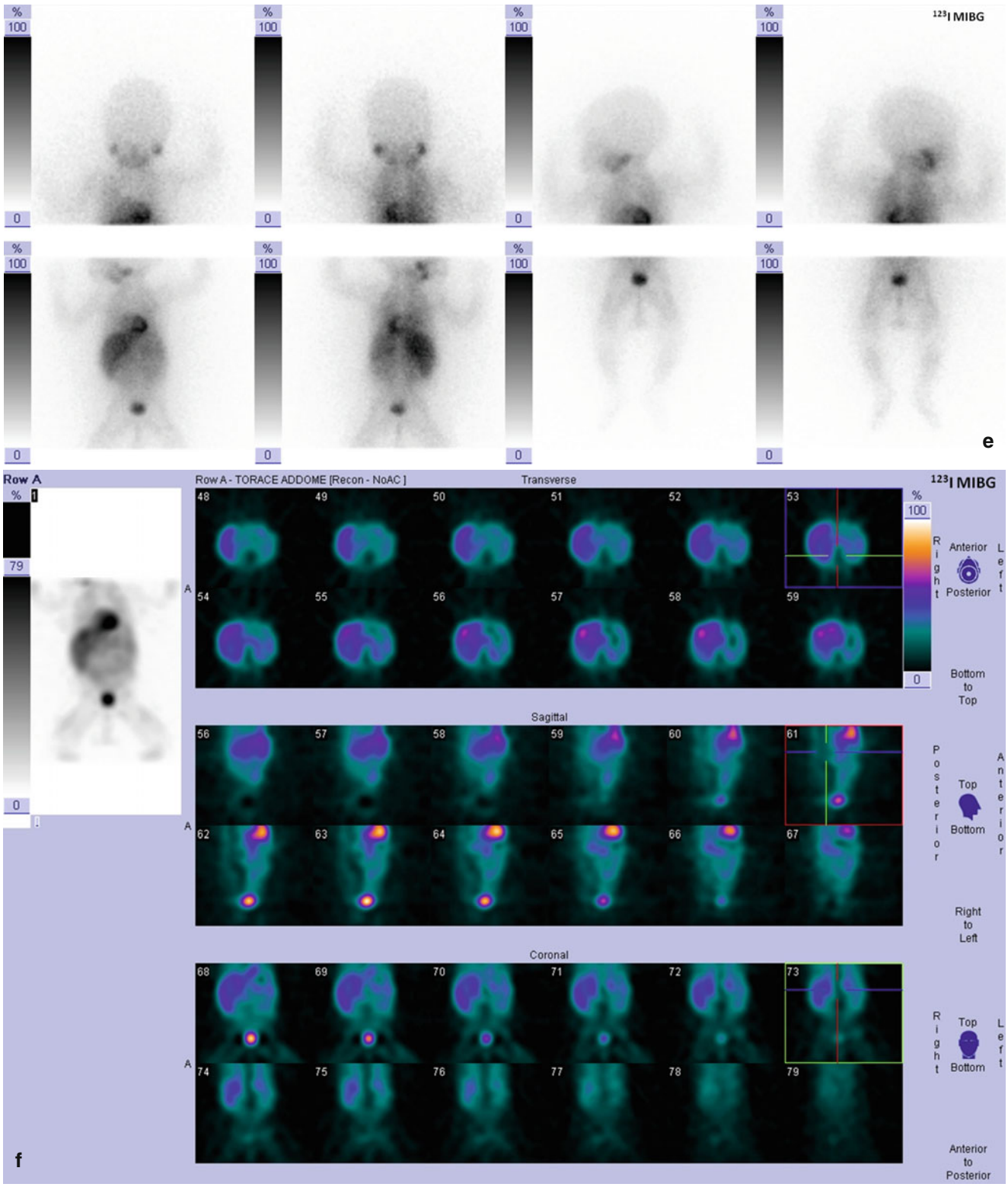

Fig. 13.2 (continued)

13.2.3 Case 13.3: MIBG Scintigraphy in Localized Thoracic Neuroblastoma Infiltrating Spinal Canal

An 11-month-old baby presents sudden hypotonia and difficulty in crawling; physical examination confirms hypotonia of the lower limbs. Suspecting a spinal cord compression, a brain and spine magnetic resonance (MR) (Fig. 13.3a–d) and a chest and abdomen computed tomography (CT) (Fig. 13.3e,f) are performed, and a left mediastinal mass is detected localized at the costovertebral junction between the T1 and T6 spinal levels, with foraminal and intraspinal extension. Histological examination shows a stroma-poor NB, and, subsequently, a MIBG scintigraphy for staging purpose is scheduled and confirms the presence of the mass without metastases (Fig. 13.3g, h). Genomic profile shows absence of numerical chromosomal aberration, and so the case is defined as L2 neuroblastoma <12 months of age at diagnosis with IDRFs – NCA genomic profile with life-threatening symptoms. Patient is enrolled in LINES protocol – Group 2, and underwent chemotherapy. After receiving two courses of chemotherapy with carboplatin and etoposide, a complete resolution of symptoms is observed. A re-evaluation of disease shows the persistence of IDRFs; so, patient undergoes follow-up.

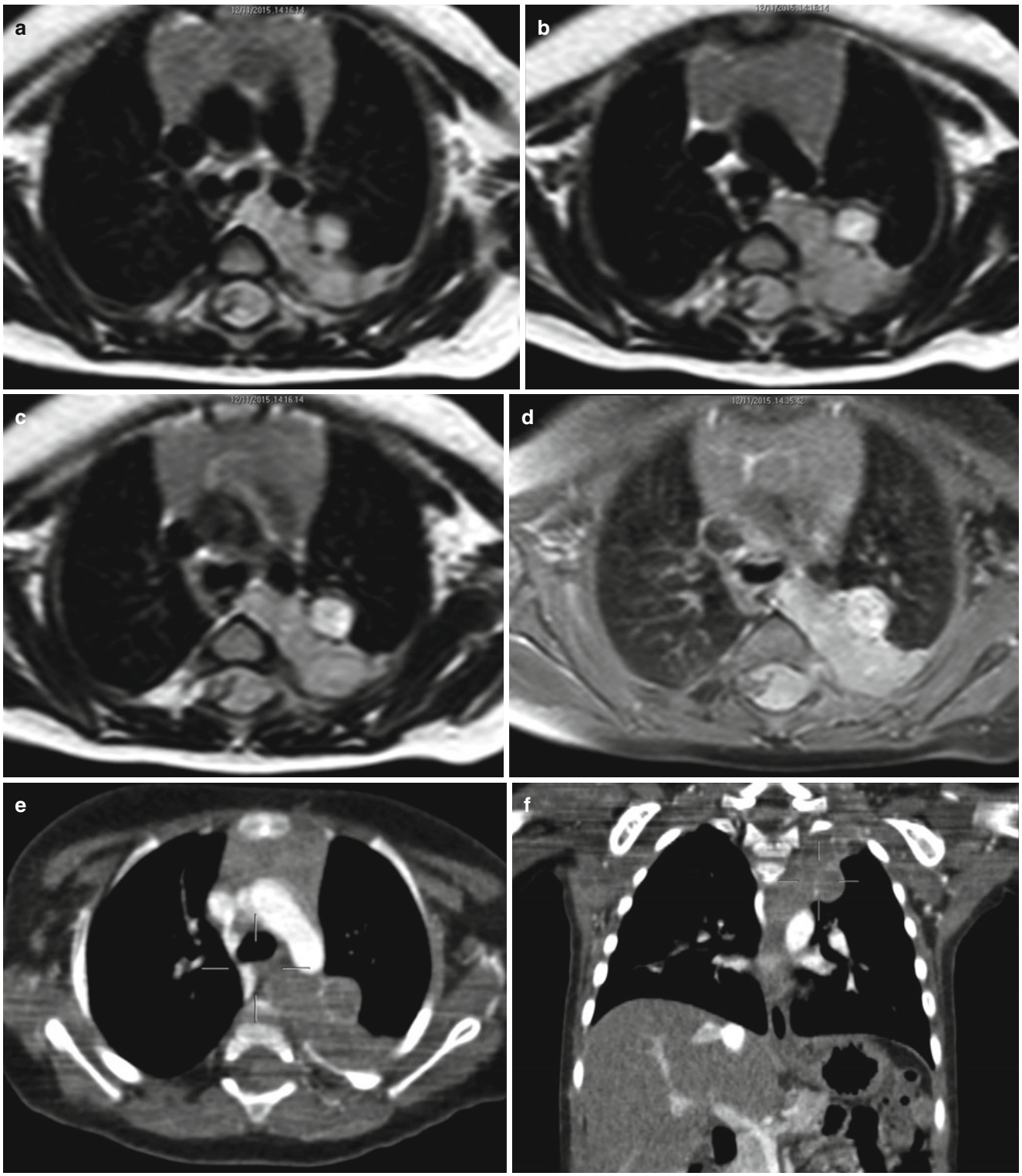

Fig. 13.3 (**a**–**f**) Transverse nonenhanced T2-weighted MR image and postcontrast T1-weighted image (**a**–**d**), and transverse and MPR coronal contrast-enhanced CT (**e**, **f**) imaging show left mediastinal mass localized at the costovertebral junction between T1 and T6 spinal levels, with foraminal and intraspinal extension (dumbbell tumor). A "contact" is present between the lesion and the aorta (aortic arch and descending aorta), the left subclavian vein, and the azygous vein, respectively. In postcontrast imaging (both CT and MRI), more than one-third of the spinal canal in the transverse plane is invaded, and the leptomeningeal spaces are not visible; the spinal cord MR signal intensity appears altered, as for marrow infiltration. (**g**, **h**) MIBG scintigraphy (static views, **g**) shows an area of intense and nonhomogeneous radiotracer uptake in the posterior chest; SPECT-CT fused images (**h**) confirm that the area of uptake corresponds to the mass detected by CT; no other areas of pathological uptake of radiotracer are evident

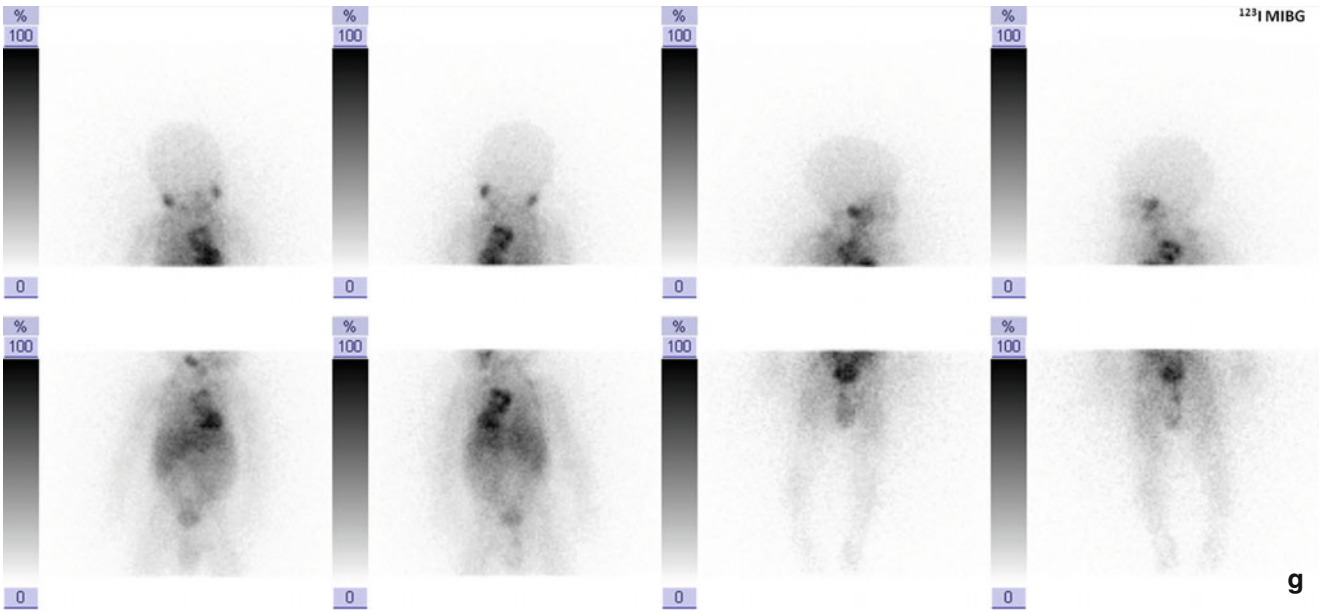

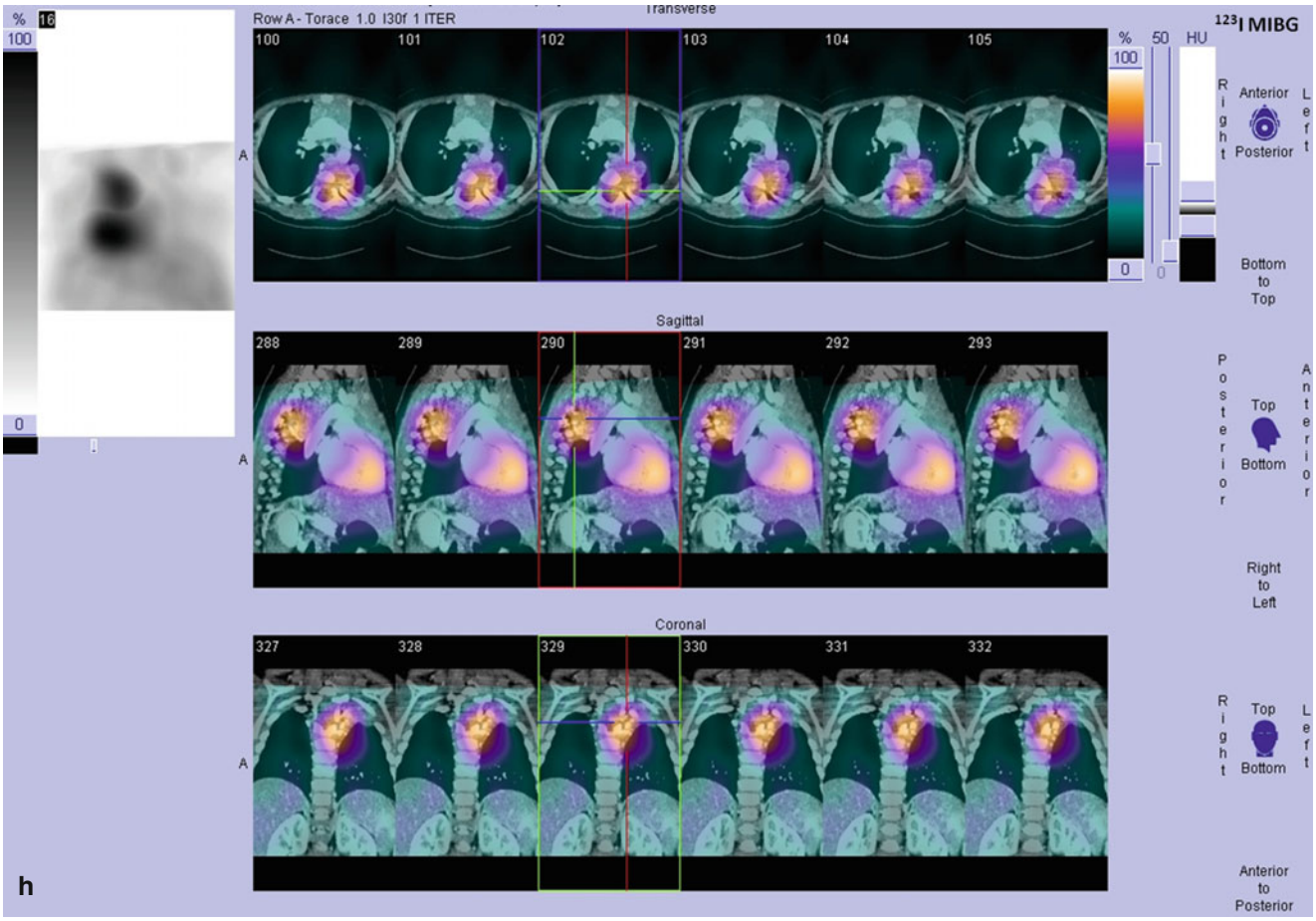

Fig. 13.3 (continued)

13.2.4 Case 13.4: MIBG Scintigraphy in Localized Abdominal Neuroblastoma

A 5-month-old baby undergoes an ultrasonography for incidental finding of abdominal swelling; US shows a solid lesion localized in the left retroperitoneal space on the middle line. CT detected a large retroperitoneal, prevertebral mass, with some calcifications (Fig. 13.4a–c), and suspected for NB, confirmed by histological examination (NB stroma poor). Subsequently, MIBG scan is scheduled for staging purpose and detects the presence of the mass without metastases (Fig. 13.4d, e).

Genomic profile shows the absence of numerical chromosomal aberration; so, the case is defined as L2 neuroblastoma <12 months of age at diagnosis with IDRFs – NCA genomic profile without life-threatening symptoms. Patient is enrolled in LINES protocol – Group 1 and randomized to receive chemotherapy.

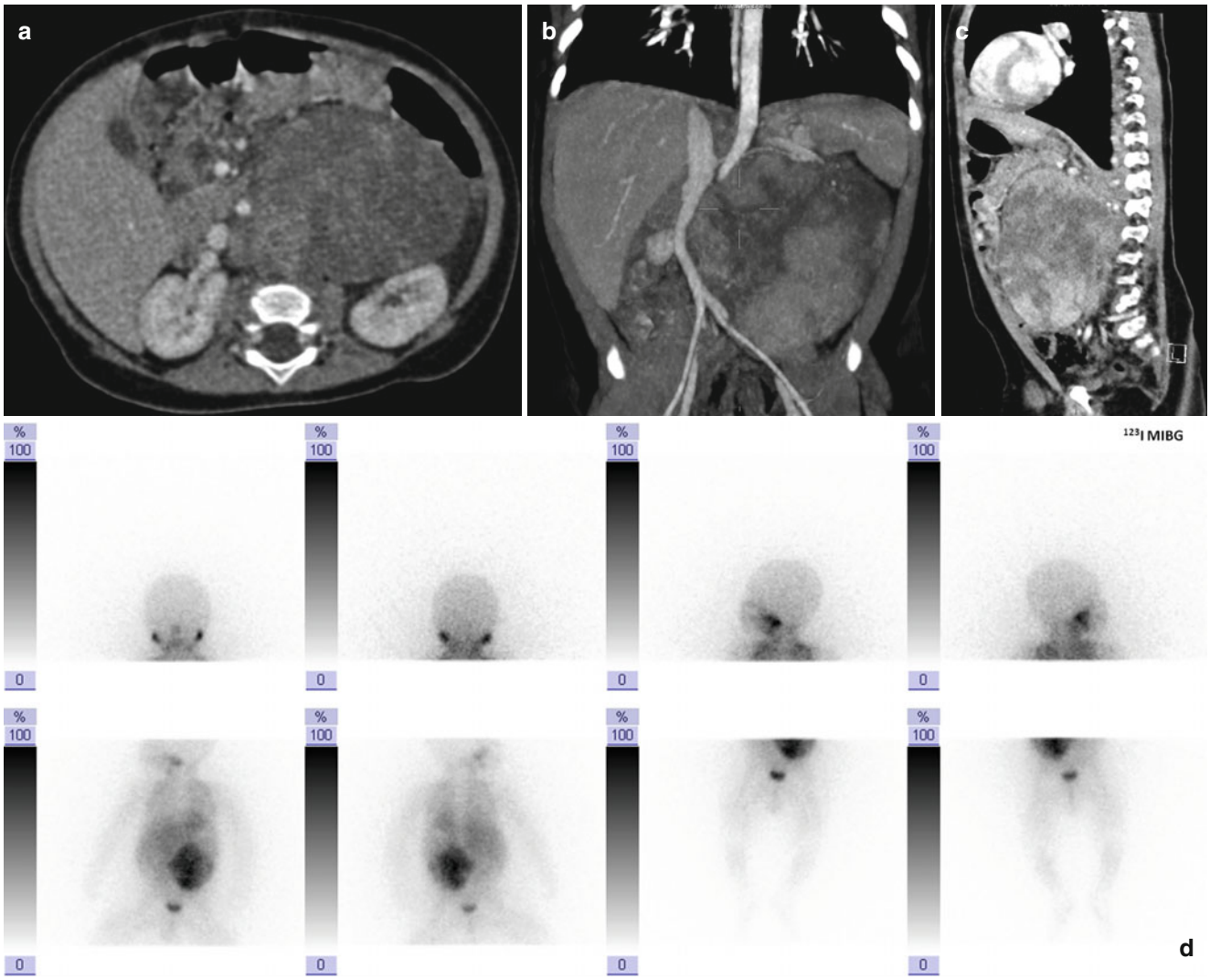

Fig. 13.4 (**a**–**c**) Contrast-enhanced CT. Transverse (**a**), MPR coronal (**b**), and sagittal (**c**) images show a large tumor in left abdomen, crossing the midline, containing large areas of amorphous calcifications, with nonhomogeneous enhancement after contrast media administration. Left kidney is displaced and distorted by the tumor but not infiltrated, as the normal cortex is still visible; aorta and inferior cava are pervious, although stretched, flattened, and displaced anteriorly, such as celiac artery, hepatic artery, and superior mesenteric vessels. Tumor infiltrates the iliolumbar fossa, without foraminal and intraspinal extensions. (**d**, **e**) MIBG scintigraphy (static views, **d**) detects a large area of intense and nonhomogeneous radiotracer uptake in abdomen-pelvis, crossing the middle line; SPECT-CT fused images (**e**) confirm that the area of uptake corresponds to the mass detected by CT; no other areas of pathological uptake of radiotracer are evident

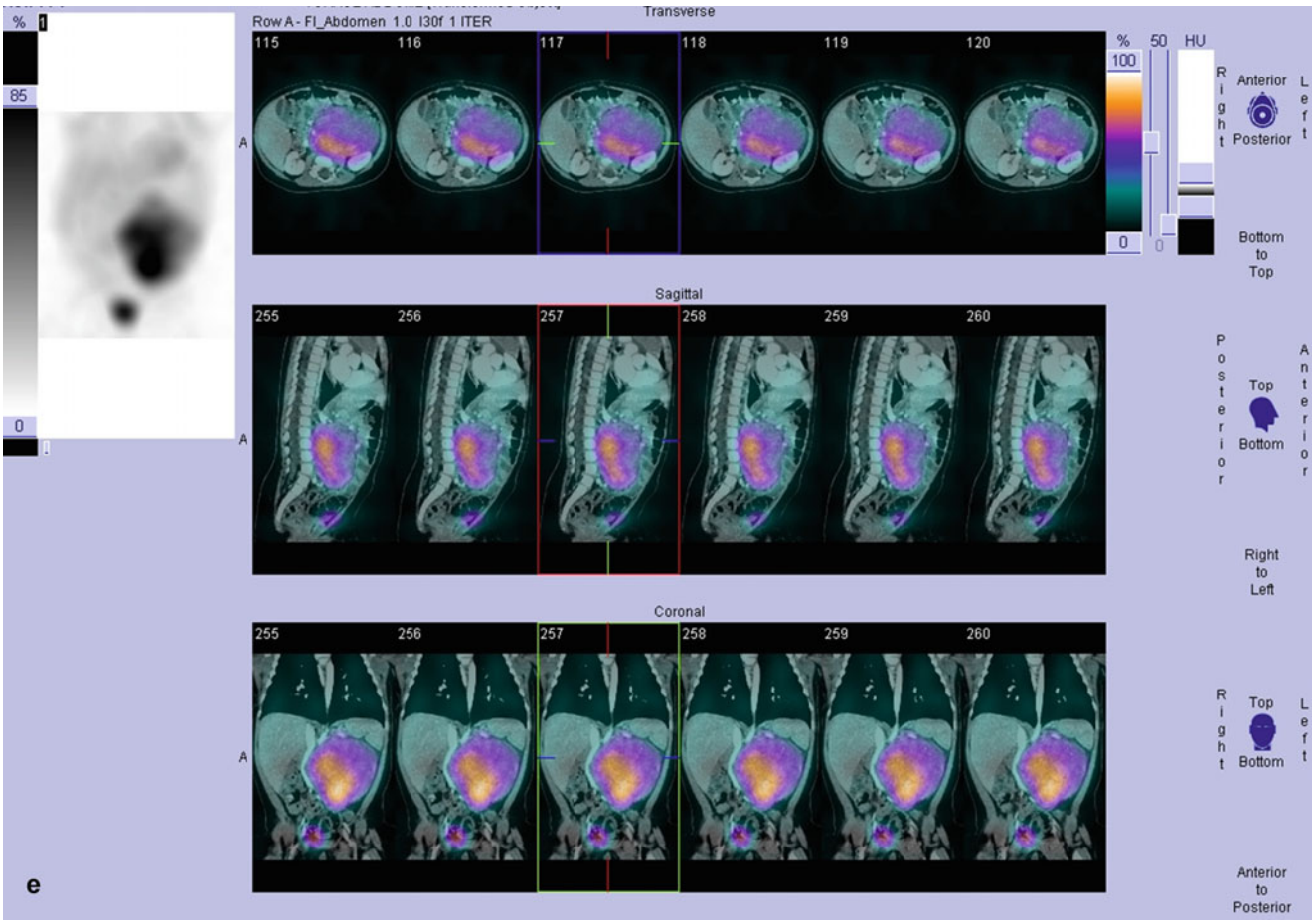

Fig. 13.4 (continued)

13.2.5 Case 13.5: MIBG Scintigraphy in MS Neuroblastoma

A 2-month-old baby refers to our institution for vomiting and lack of appetite; an ultrasonography shows a left adrenal lesion that compresses left kidney and multiple hyperechoic areas in the liver, respectively. CT confirms ultrasonographic findings (Fig. 13.5a–f).

Histological examination reveals a NB; therefore, the baby undergoes a MIBG scan for staging purpose (Fig. 13.5g, h); scintigraphy detects the mass and a nonhomogeneous radiotracer uptake in the liver, due to the presence of metastases; no other areas of pathological uptake of radiotracer are evident.

Genomic profile shows the absence of segmental chromosomal aberration; so, the case is defined as MS neuroblastoma without SCA and without life-threatening symptoms. The patient is enrolled in LINES protocol – Study arm low-risk MS.

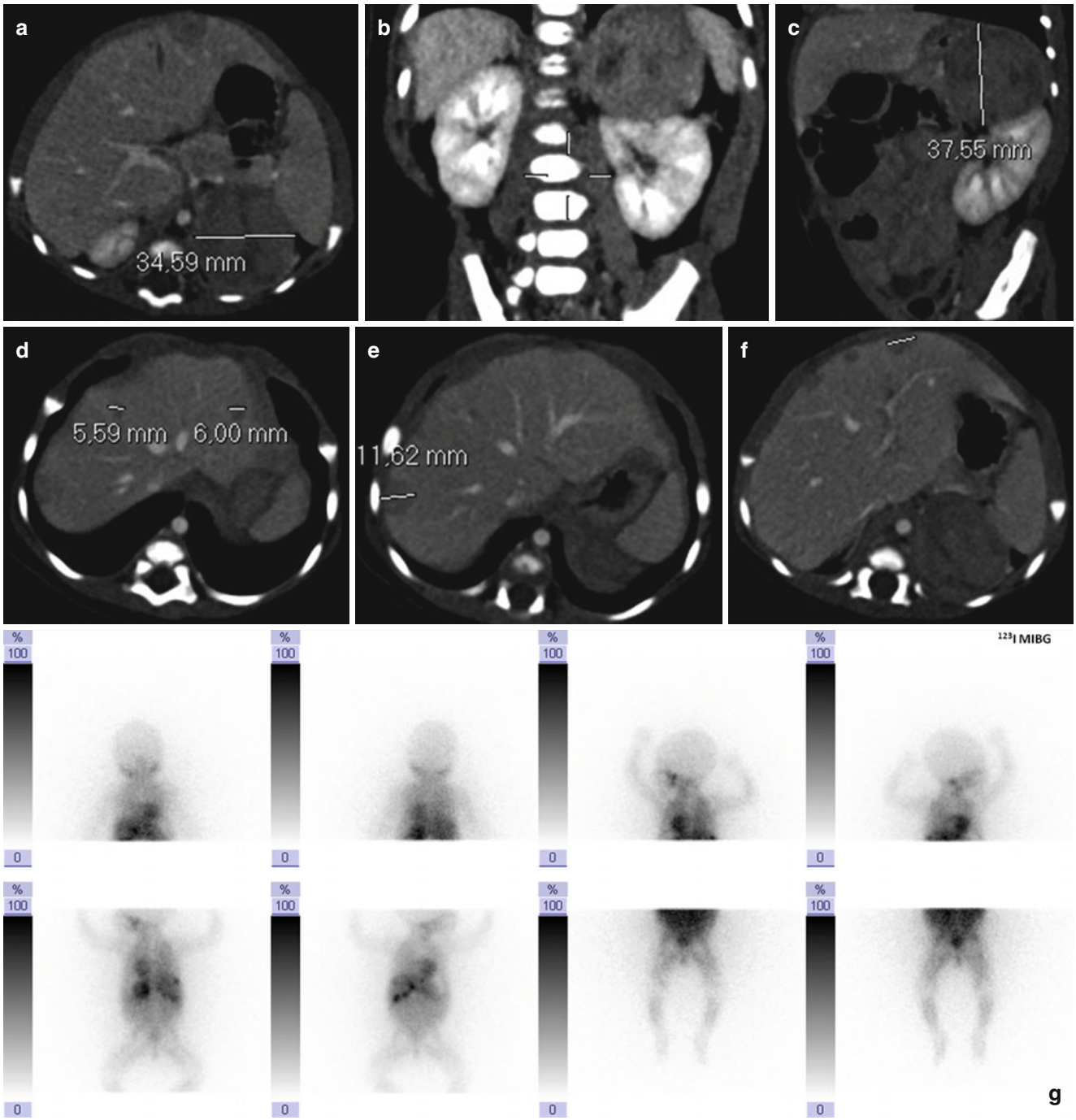

Fig. 13.5 (**a**–**f**) Contrast-enhanced CT. Transverse (**a**), MPR coronal (**b**), and sagittal (**c**) images show a mass in left adrenal lodge (with diameters about 41×35×38 mm); tumor appears round-shaped and well-circumscribed; it displaces and compresses left kidney, separated from the tumor by a fatty layer. The mass has a wide contact with aorta, celiac artery, and splenic vessels, stretched and flattened; a part of the left vein is completely encased by the tumor. CT scan shows also multiple peripherally enhancing lesions throughout the liver, consistent with the metastases (transverse images, **d**–**f**). (**g**, **h**) MIBG scintigraphy (static views, **g**) detects a large area of intense and nonhomogeneous radiotracer uptake in abdomen, in left paravertebral region; SPECT-CT fused images (**h**) confirm that the area of uptake corresponds to the adrenal lesion detected by CT; the liver shows nonhomogeneous radiotracer uptake, due to multiple secondary nodules evident at CT (**g**, **h**); no other areas of pathological uptake of radiotracer are evident

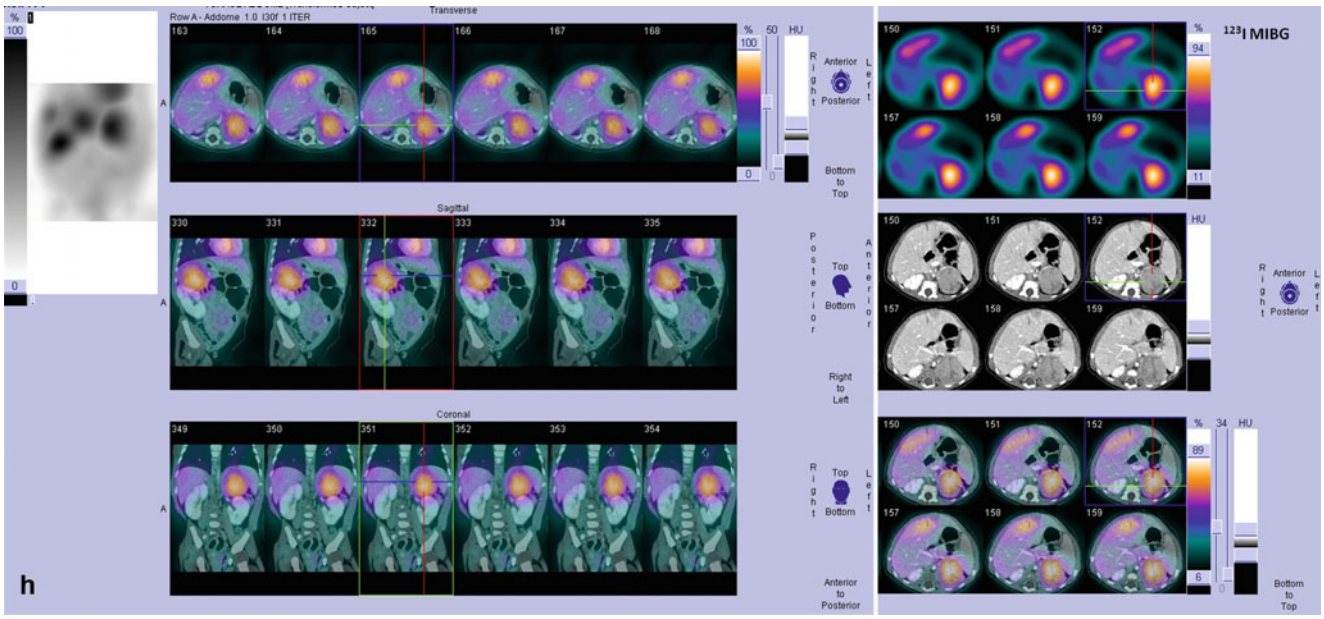

Fig. 13.5 (continued)

13.2.6 Case 13.6: Infant Stage IV Neuroblastoma: MIBG and Bone Scan Imaging Integration

A 2-month-old baby refers to our institution for appearance of multiple blue nodules on the skin; an ultrasonography shows a left adrenal mass that compresses left kidney and multiple hyperechoic areas in the liver. CT detects a prevertebral mass located in the left adrenal lodge with multiple calcification and multiple hypodense areas in the liver, respectively; several nodules are also evident in subcutaneous fat tissue of chest, abdomen, and pelvis; no lesions are evident in the skeleton (Fig. 13.6a–f). Histological examination of one of this nodules reveals a metastasis of NB; therefore, the baby undergoes a MIBG scan for staging purpose (Fig. 13.6g); scintigraphy shows a MIBG-avid mass and a nonhomogeneous radiotracer uptake in the liver, due to the presence of metastases; multiple areas of focal radiotracer uptake are evident in the abdomen, in the pelvis, and in the lower limbs (corresponding to known skin lesions).

Moreover, two focal areas of MIBG uptake are evident in the right orbital region and in the left proximal humerus, respectively; it has been considered that these two foci of uptake are probably due to bone metastasis.

For this reason, the child undergoes 99Tc-MDP bone scan (Fig. 13.6h) that shows uptake of radiotracer in the right orbital region, corresponding to MIBG uptake.

Chemotherapeutic treatment is carried out, and MIBG scintigraphy after chemotherapy (Fig. 13.6i) shows persistence of MIBG uptake in the primitive lesion and known skin lesions; nonhomogeneous radiotracer uptake in the liver is still present. Uptake in bone is no longer evident, such that indicating response to chemotherapy of the bone lesions.

The girl then undergoes surgery on primary NB, and is followed up with laboratory examination and periodic CT and MIBG scan.

At last follow-up, MIBG scintigraphy (Fig. 13.6j shows a single, very small area of faint MIBG uptake in one of the known skin lesions and nonhomogeneous uptake in the liver.

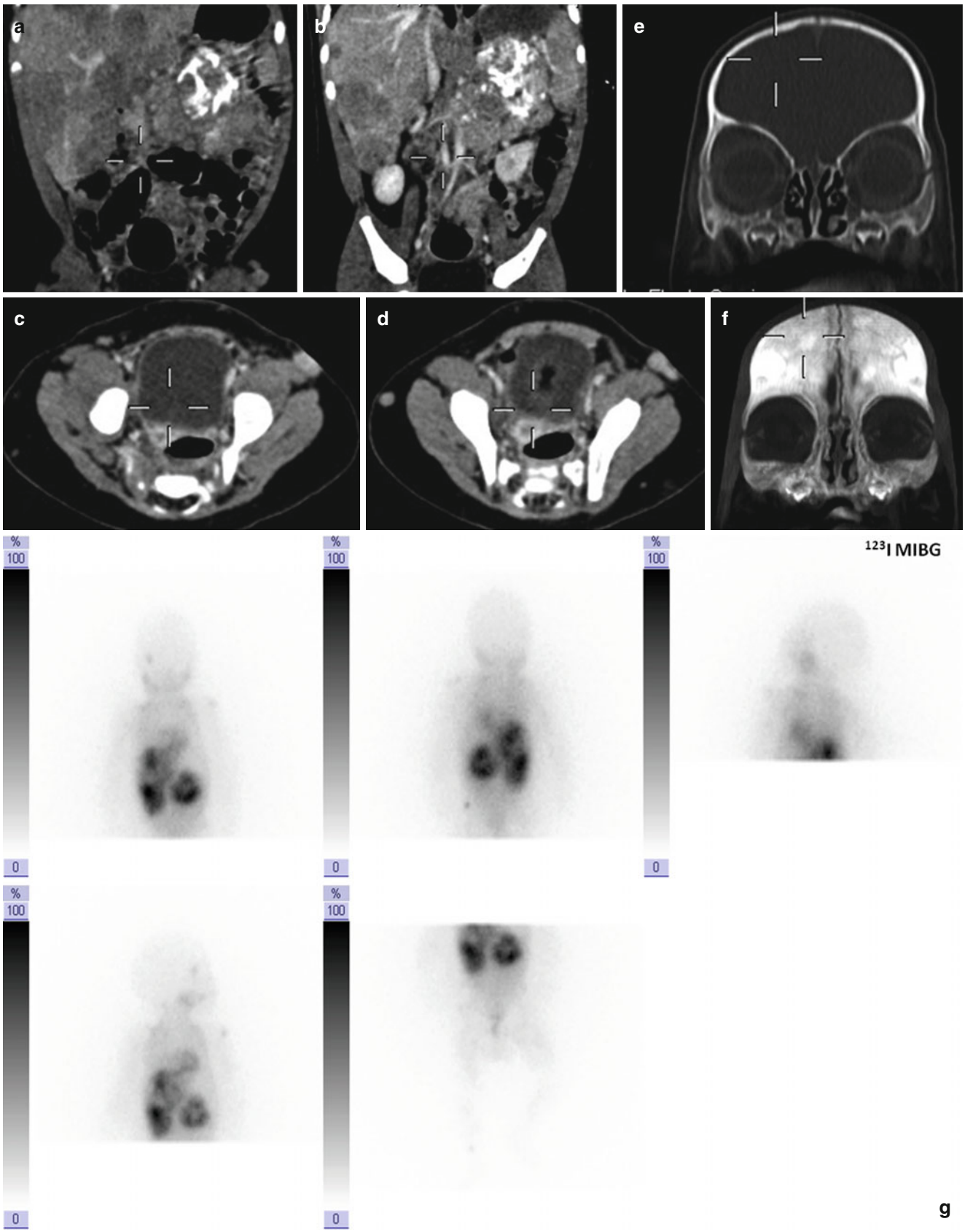
a
b
e
c
d
f
%
100
0
123I MIBG
g

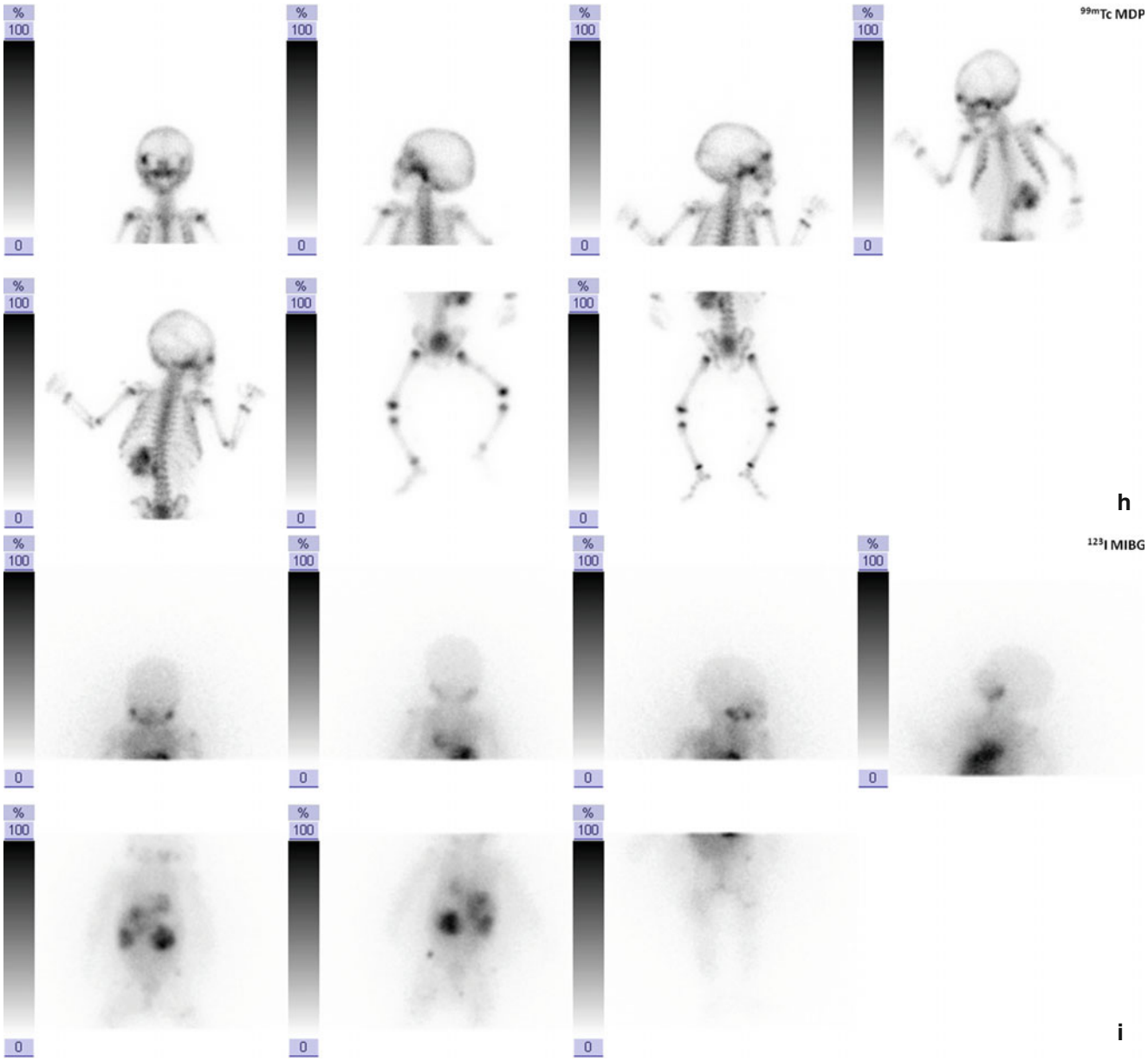

Fig. 13.6 (continued)

Fig. 13.6 (**a**–**f**) Contrast-enhanced CT. MPR coronal (**a**, **b**) and transverse (**c**, **d**) images show a nonhomogeneous and aggressive retroperitoneal mass containing many amorphous calcifications and located in the area of the left adrenal gland; the mass does not infiltrate the kidney and was about 40×35×48 mm in size. Many lymph node metastases, multiple subcutaneous nodules, and liver enhancing lesions are also seen. Head CT scan (**e**, **f**) does not show images consistent with metastases. (**g**) Staging MIBG scintigraphy (static views) detects a large area of intense and nonhomogeneous radiotracer uptake in abdomen, in left paravertebral region, corresponding to the lesion showed by CT that does not cross the middle line; the liver shows nonhomogeneous radiotracer uptake, due to multiple secondary nodules evident at CT; multiple areas of focal radiotracer uptake are evident in proximal region of left humerus, in abdomen, in the pelvis, and in lower limbs (corresponding to known skin lesions). A focal area of radiotracer uptake is evident in the right orbital region, suspected for bone metastases. (**h**) 99Tc-MDP bone scan (static views) shows focal uptake of radiotracer in the right orbital region, corresponding to MIBG uptake. Faint uptake is evident in known skin lesions; intense uptake of radiotracer is also evident in abdominal mass (frequent in NB, due to the presence of calcifications). (**i**) MIBG scintigraphy after chemotherapy (static views) shows persistence of intense radiotracer uptake in abdomen, in the primitive lesion, and of nonhomogeneous radiotracer uptake in the liver, respectively; focal uptake in known skin lesions is still present, while radiotracer uptake in right orbital region and in left proximal humerus is no longer evident, such indicating response to chemotherapy of the bone lesions. (**j**) MIBG scintigraphy during follow-up (static views) shows a single, very small area of faint extraskeletal radiotracer uptake in soft tissue of left iliac region (corresponding to known skin lesion) and nonhomogeneous uptake in the liver

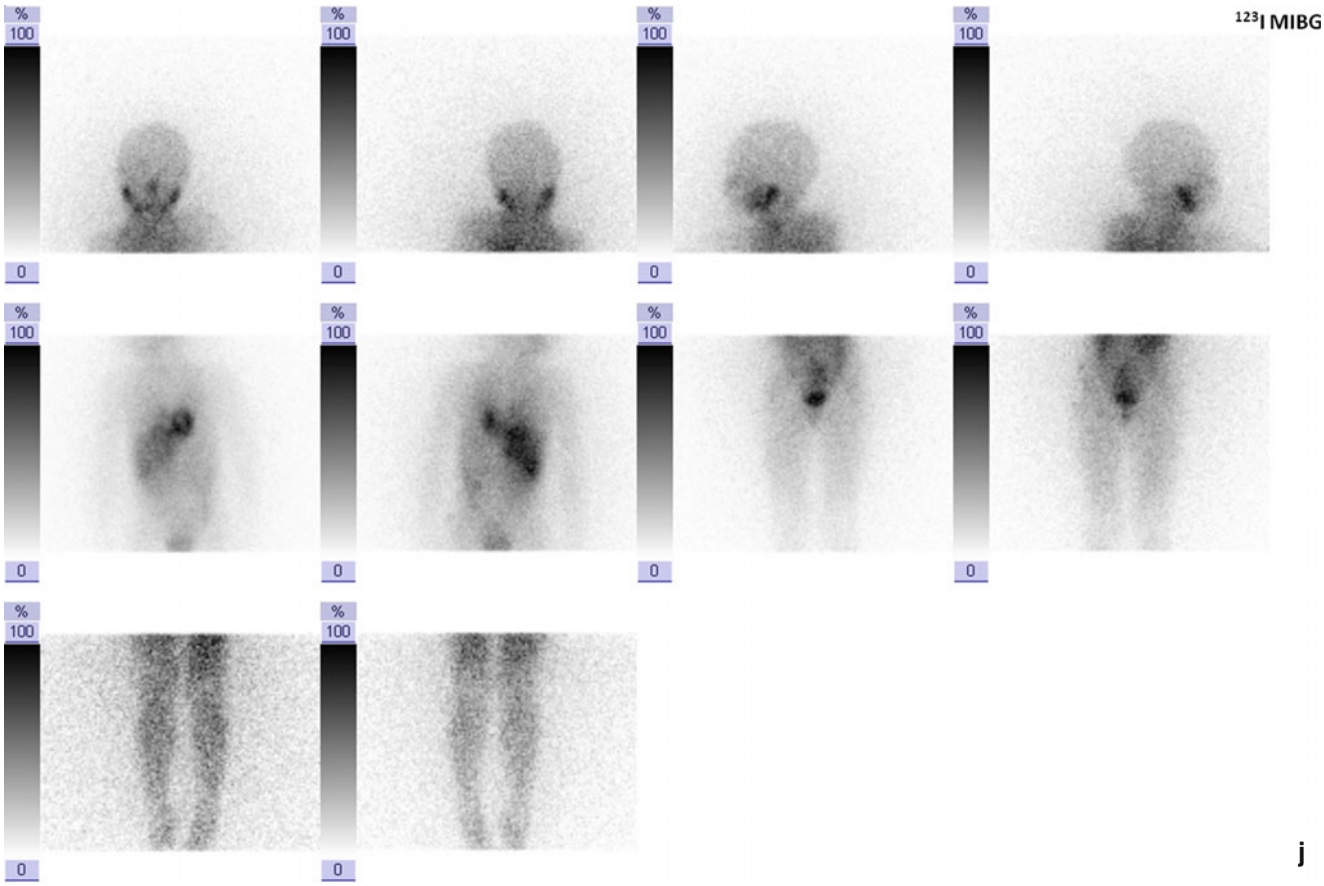

Fig. 13.6 (continued)

13.2.7 Case 13.7 MIBG Scintigraphy in Localized Abdominal Ganglioneuroma/ Ganglioneuroblastoma

A 7-year-old girl refers to our institution for abdominal pain; an ultrasonography shows a left adrenal mass that dislocates left kidney; CT confirms a solid mass with calcifications that impresses the upper pole of the left kidney, suspected for NB (Fig. 13.7a–c). The girl undergoes 123I-MIBG scintigraphy to confirm the suspicion (Fig. 13.7d, e), and the lesion appears as nonavid of MIBG. Subsequently, a biopsy of the lesion is performed, and histological examination shows a peripheral neuroblastic tumor, borderline between ganglioneuroma "maturing" and intermixed ganglioneuroblastoma, such that explaining the absence of MIBG uptake.

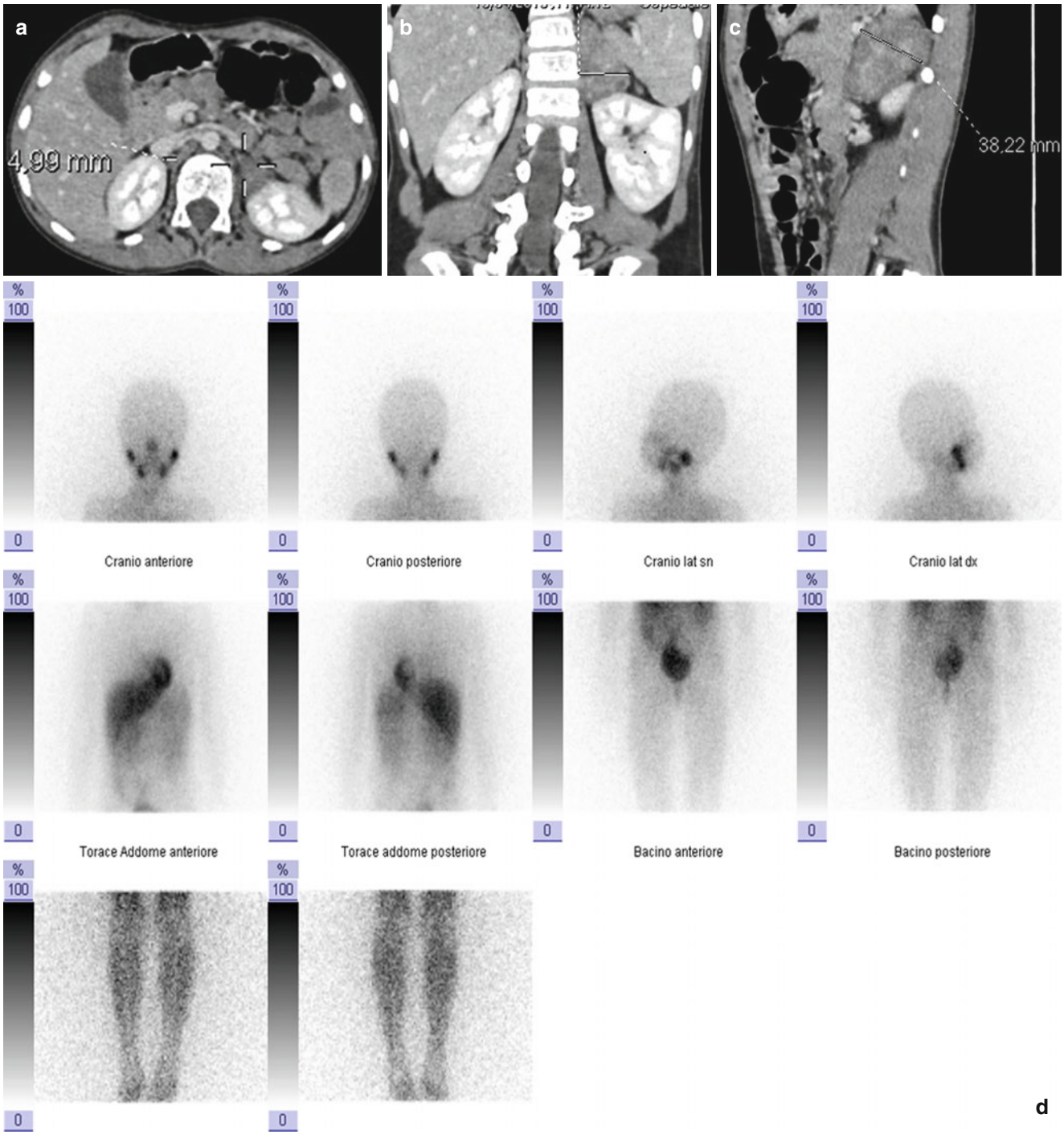

Fig. 13.7 (**a**–**c**) Contrast-enhanced CT. Transverse (**a**), MPR coronal (**b**), and sagittal (**c**) images show a large mass in the left suprarenal region (about 58 × 28 × 39 mm in diameter). The lesion, containing tiny dystrophic calcifications, is oval-shaped and shows nonhomogeneous enhancement after contrast agent administration. Left kidney is inferiorly displaced; left adrenal gland, pancreatic tail, and medial border of the spleen are also displaced, although separated from the tumor by a fatty layer. (**d**, **e**) MIBG scintigraphy (static views, **d**) does not show any area of uptake of radiotracer; in particular, the lesion detected by CT appears as nonavid of MIBG. SPECT-CT fused images (**e**) confirm this finding

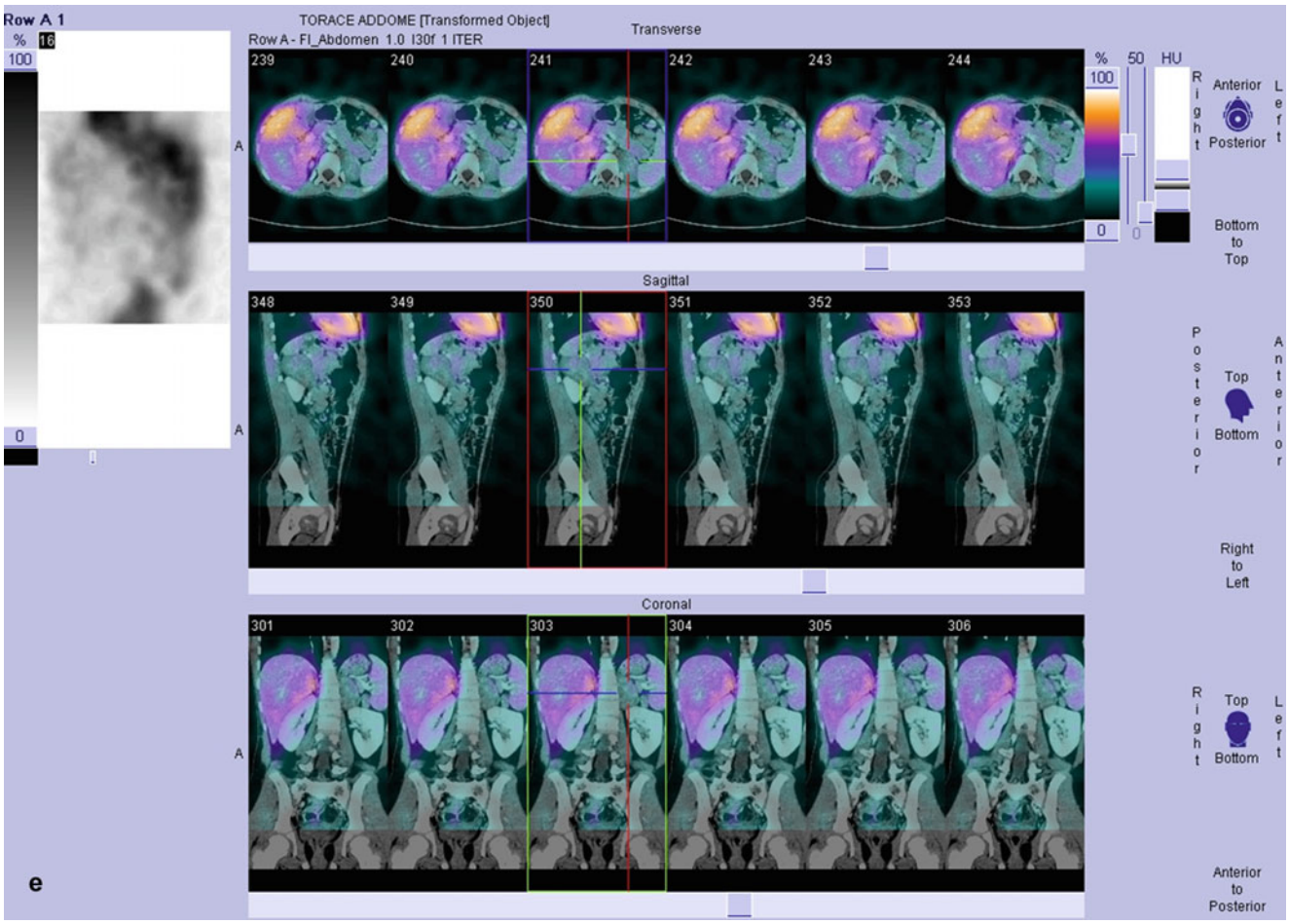

Fig. 13.7 (continued)

13.2.8 Case 13.8 MIBG Scintigraphy in Localized Thoracic Neuroblastoma Without Involvement of Spinal Canal

A 3-year-old girl presents persistent cough since 1 month; she received specific therapy, but because of the persistence of symptom, a chest radiography, a CT scan, and a MR (Fig. 13.8a–c) are performed, and neoplasia is detected in the posterior mediastinum, suspected for NB. For this reason, the girl undergoes 123I-MIBG scintigraphy (Fig. 13.8d, e), which shows intense radiotracer uptake in the mass, without evidence of metastases.

To better characterize the neoplasia, a biopsy was performed, and diagnosis of differentiating ganglioneuroblastoma nodular performed. Patient was treated according to LINES protocol, and then the tumor was completely resected.

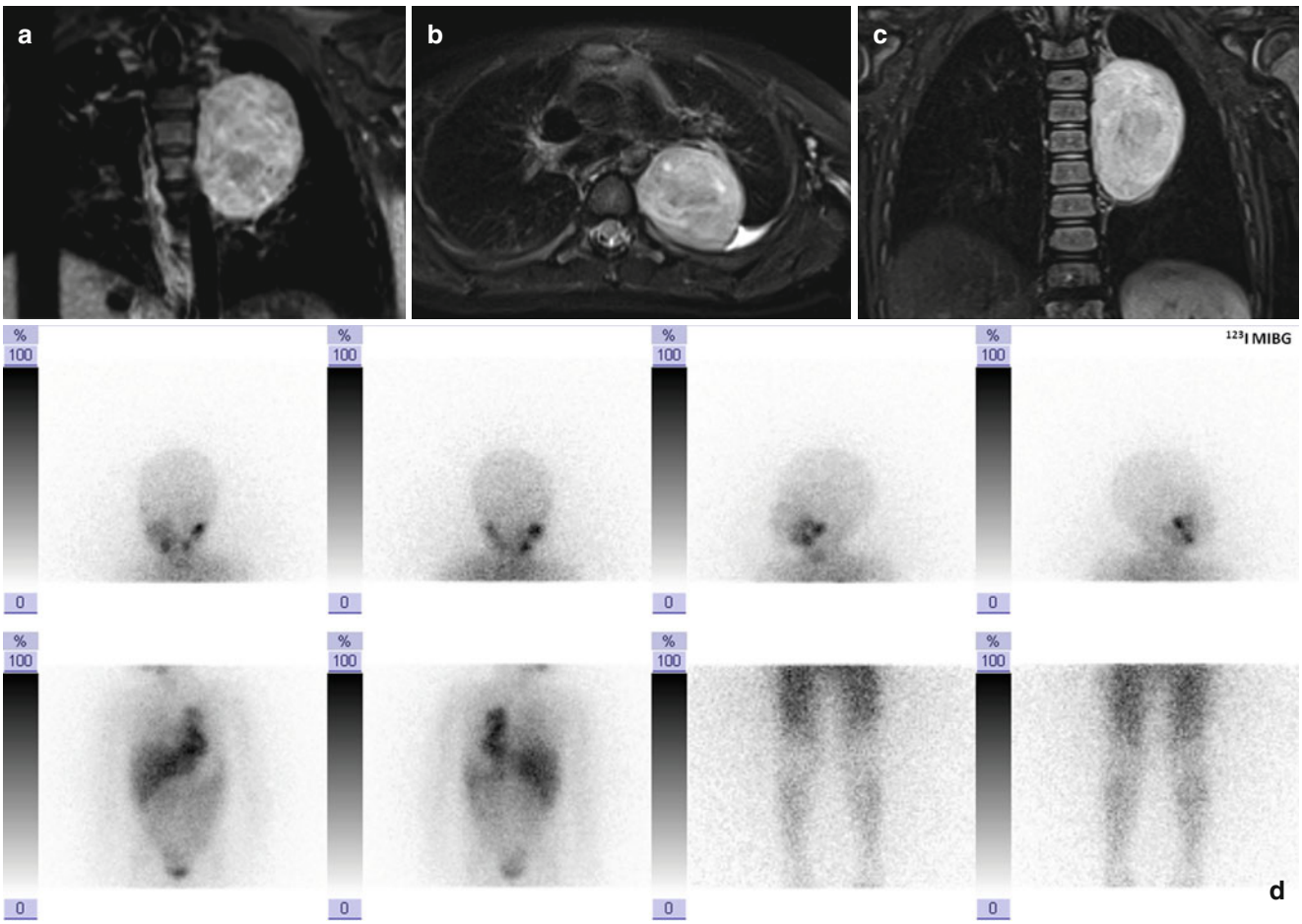

Fig. 13.8 (**a**–**c**) TransverseT2-weighted fat-sat (**a**), coronal T2-weighted TIRM (**b**), and postcontrast transverse T1-weighted MR images show a large, left upper posterior mediastinal mass; it is localized between T3 and T8 spinal levels, and it does not show foraminal and intraspinal extensions. A "contact" is present between the lesion and the descending aorta, without signs of infiltration of the nearest anatomical structures. (**d**, **e**) MIBG scintigraphy (static views (**d**) detects a large area of intense radiotracer uptake in the chest, corresponding to large mass in posterior mediastinum, in paravertebral region, corresponding to the lesion showed by MRI, as better evident on SPECT-MRI fused images (**e**)

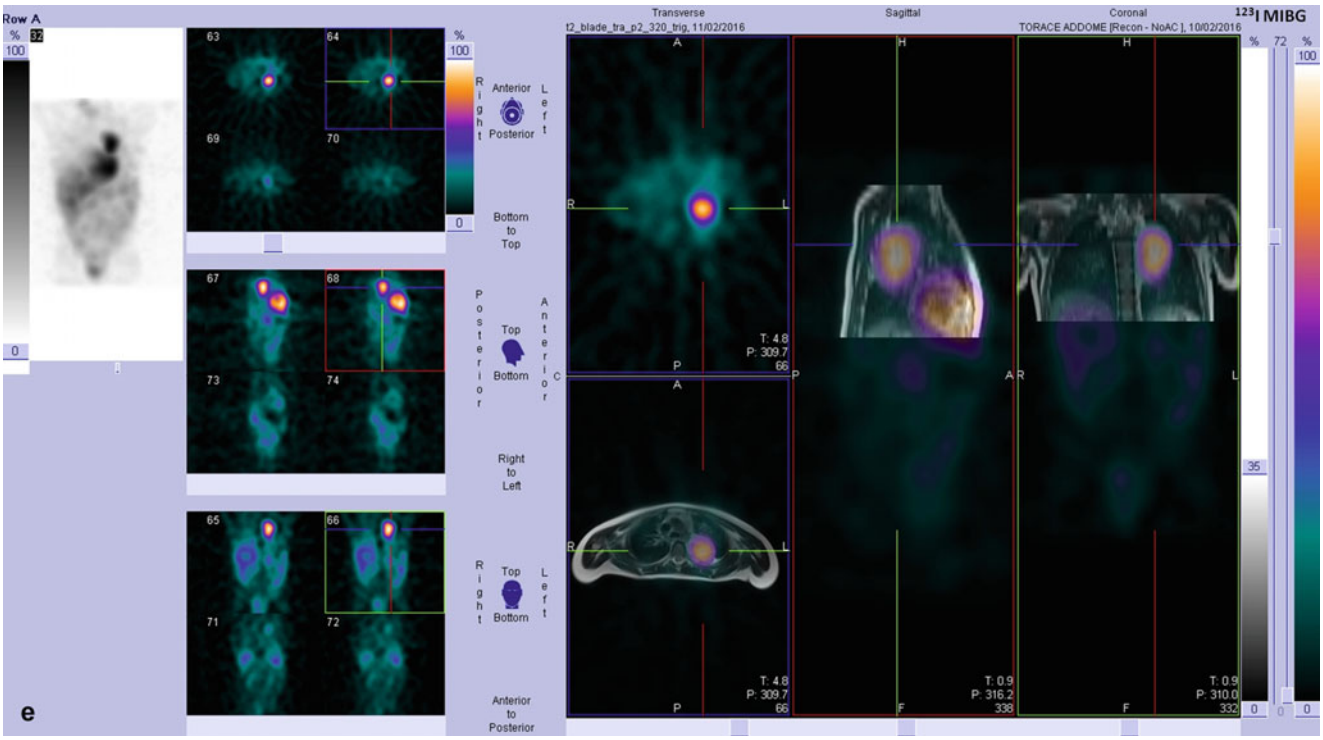

Fig. 13.8 (continued)

13.2.9 Case 13.9 Stage IV NB: Scintigraphic Evidence of Complete Response to Induction Chemotherapy in Metastatic Sites

A 5-year-old girl refers to our institution for pain in pelvis and lower limbs; at clinical evaluation, the girl presents a hard swelling in abdomen. Therefore, an abdominal US and a subsequent CT are performed, and a large mass in the abdomen is detected (Fig. 13.9a, b), suspected for NB; histological examination confirms the diagnosis (NB stroma poor), and a MIBG scintigraphy is scheduled as part of diagnostic workup; the scan detects spread of disease in the bone and bone marrow, as well as the mass (Fig. 13.9c). Genomic profile shows NMYC not amplified. Patient is treated according to NBHR01 European protocol and patient randomized to N7 arm.

At the end of induction treatment, a new balance of disease by CT scan, bone and bone marrow biopsy, and MIBG scan is performed. The CT scan showed a partial response of primary tumor (Fig. 13.9d, e); bone and bone marrow biopsy are negative for infiltration of disease; MIBG scintigraphy shows disappearance of metastatic disease (Fig. 13.9f).

Fig. 13.9 (**a**, **b**) MPR coronal contrast-enhanced computed CT shows large retroperitoneal mass (**a**), with nonhomogeneous density after contrast agent administration and tiny peripheral calcifications. The lesion, oval-shaped, with irregular borders, displaces anteriorly the pancreatic gland and the superior mesenteric artery. There are also multiple metastatic nodes with inner coarse calcifications located in retroperitoneal fatty space and extending along iliac vessels both on the right and on the left. CT scan does not show images consistent with bone metastases (**b**). (**c**) Staging MIBG scintigraphy (static views, **c**) shows nonhomogeneous uptake in large tumor in abdomen; multiple areas of uptake are evident in skull, skull base, both orbits, sternum, many ribs in both hemithorax, in all spine, both humeri, right radius, pelvis, femurs, tibiae, and left foot, indicating bone-bone marrow involvement. (**d**, **e**) MPR coronal (**d**) and transverse (**e**) and contrast-enhanced computed tomography (CT) after chemotherapy show no significant reduction in size of the primary mass (about 52 × 82 × 45 mm), neither of the previous reported lymphadenopathies. At MIBG scintigraphy after treatment (**f**), metastatic lesions are no longer evident, while radiotracer uptake in right adrenal lodge (corresponding to residual mass) is still detectable, indicating a complete metabolic response to chemotherapy of bone and bone marrow metastasis

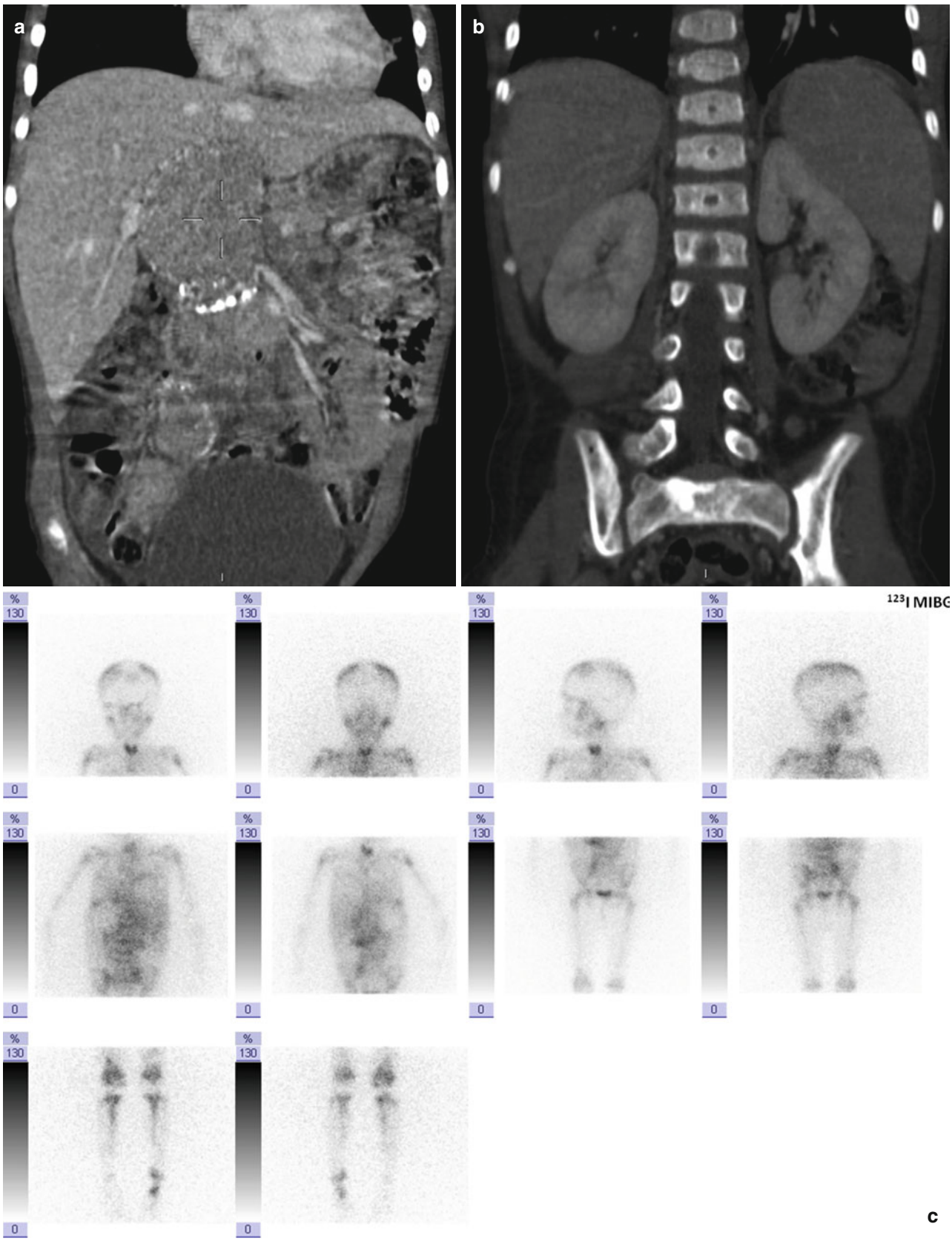
a
b
123I MIBG
c

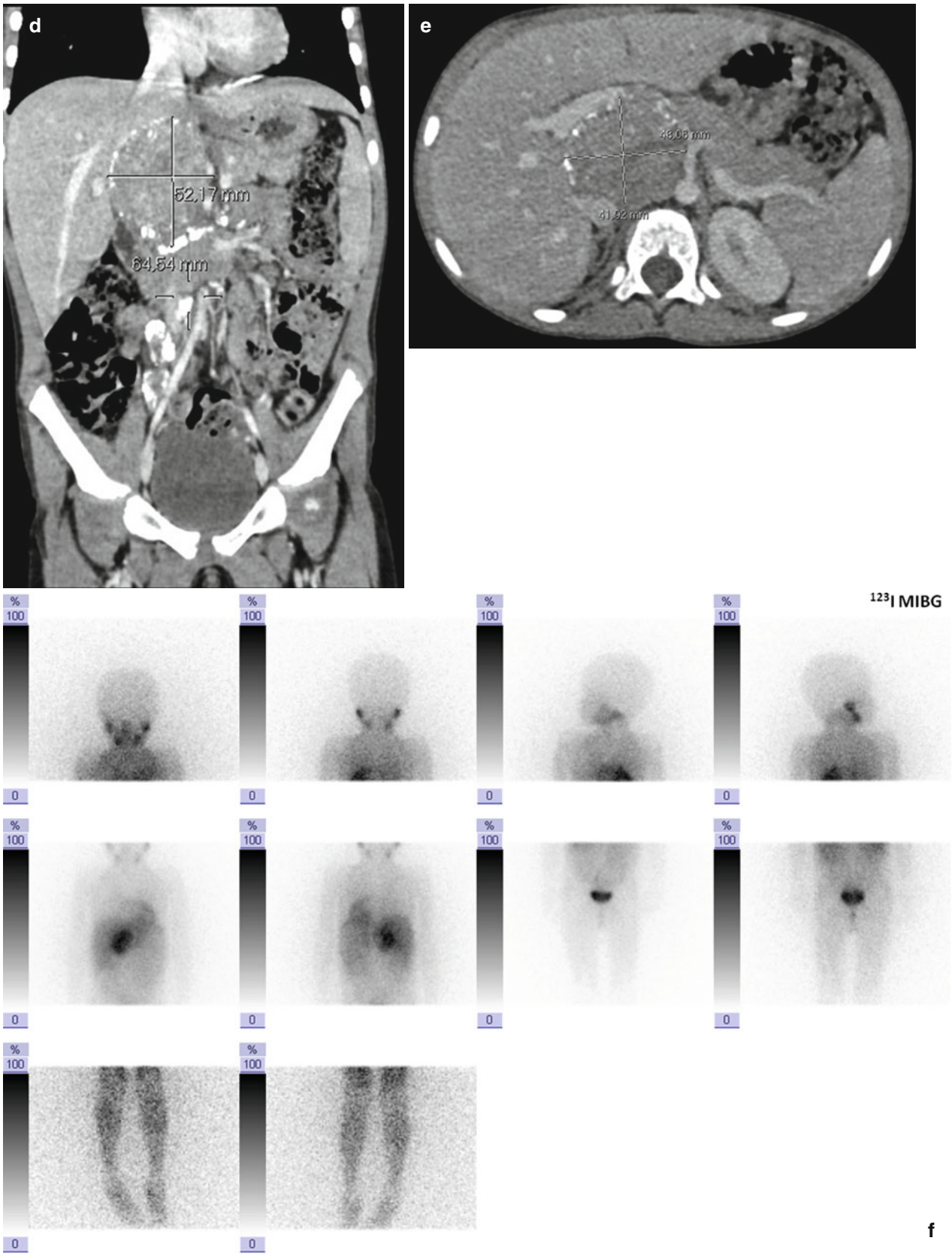

Fig. 13.9 (continued)

13.2.10 Case 13.10 Stage IV Neuroblastoma: Scintigraphic Evidence of Partial Response to Induction Chemotherapy in Metastatic Sites

A 2-year-old boy presenting limping since 1 month refers to our institution with a previous diagnosis of hip synovitis, treated with NSAI and steroid therapy; because of the persistence of symptoms, blood and biochemistry tests are performed. Blood test is normal, while biochemistry shows high level of LDH. An US is performed to check the hip synovitis, and it is extended to the abdomen, such that allowing to detect a lesion in the left adrenal gland; the next CT confirms a large tumor arising from left adrenal lodge and reaching in its distal part lumbar and sacral vertebrae; a portion of this tissue, extending from L5 to S2–S3, presents foraminal and intraspinal extension (Fig. 13.10a–c). Histological examination shows a NB stroma-poor, and MIBG scintigraphy is performed in order to complete disease staging. Scan detects spread of disease in the bone and bone marrow, as well as the mass (Fig. 13.10d). Genomic profile shows NMYC amplification.

Patient is treated according to NBHR01 European protocol and randomized to N7 arm.

At the end of induction treatment, a new balance of disease by CT scan, bone and bone marrow biopsy, and MIBG scan is performed. The CT scan shows a partial response of primary tumor (Fig. 13.10e–g); bone and bone marrow biopsy are negative for infiltration of disease; MIBG scintigraphy shows the persistence of disease in the lower limbs (Fig. 13.10h–k). For these reasons, patient receives TVD (topotecan-vincristine-doxorubicin) intensification chemotherapy regimen according to the protocol NBHR01.

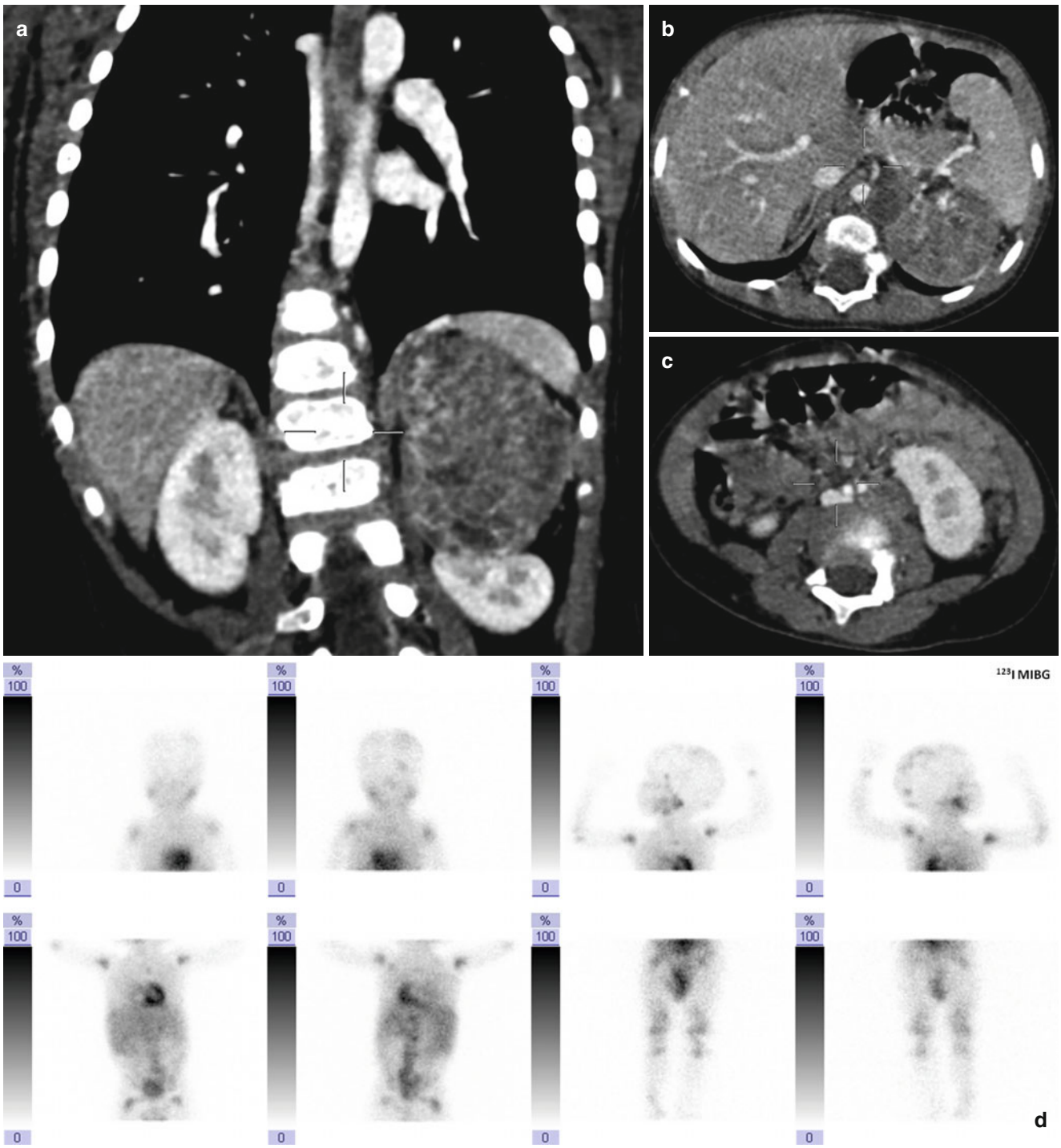

Fig. 13.10 (**a**–**c**) MPR coronal (**a**) and transverse (**b**) contrast-enhanced CT image show a large left adrenal mass, appearing at nonhomogeneously hypodense because of multiple inner nonenhancing areas after contrast agent administration. The lesion, oval-shaped, with well-defined borders, is about 51 × 43 × 62 mm in size; the left kidney is displaced and distorted but not infiltrated, as well as the spleen and the pancreatic tail. The tumor, extending in the iliolumbar fossa, invaded the spinal canal at the level between L5 and S3 via the neuroforamina (**c**). There are also multiple enlarged, metastatic retroperitoneal nodes. (**d**) Staging MIBG scintigraphy (static views) shows nonhomogeneous radiotracer uptake in the abdomen, probably corresponding to tumor evident on CT. Multiple areas of uptake are evident in skull, skull base, both orbits, sternum, left scapula, both humeri, both radii, pelvis, femurs, tibiae, and diffuse uptake in the spine, indicating bone and bone marrow involvement. (**e**–**g**) MPR (**e**) coronal and transverse (**f**) contrast-enhanced CT after treatment shows a partial response to therapy supported by a marked reduction in size of the primary mass (actually 22 × 26 × 24 mm) showing large inner calcifications. There is also a significant regression both in nodal involvement and in foraminal and intraspinal component (**g**). (**h**, **k**) MIBG scintigraphy after treatment (static views, **h**, **i**): radiotracer uptake is still evident only in distal femurs, proximal tibiae, and in right distal tibia; SPECT-CT fused images show absence of radiotracer uptake in primary tumor (**j**, **k**) and in tissue-infiltrating spinal canal. This pattern indicates a partial response to chemotherapy of bone and bone marrow lesions.

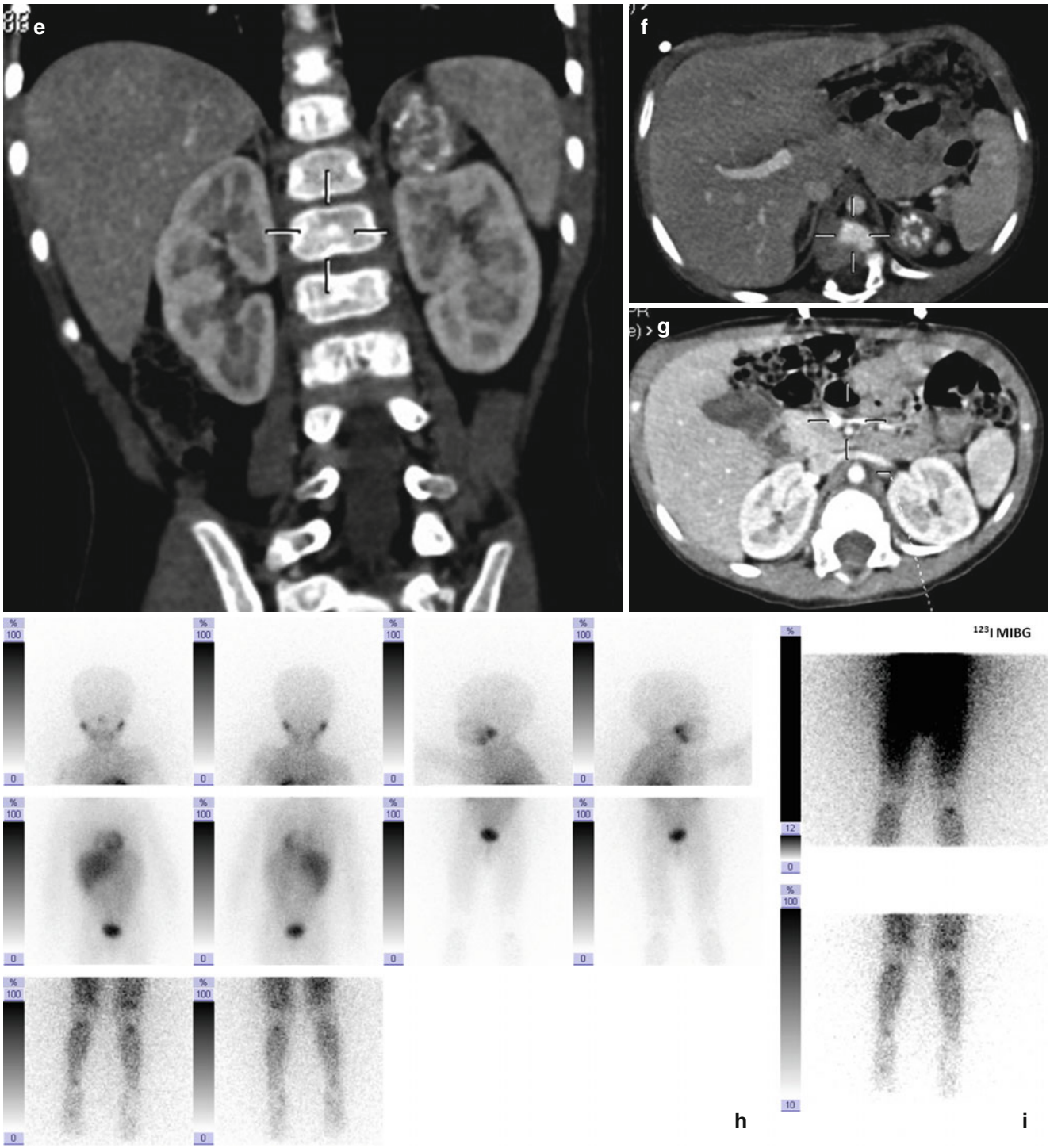

Fig. 13.10 (continued)

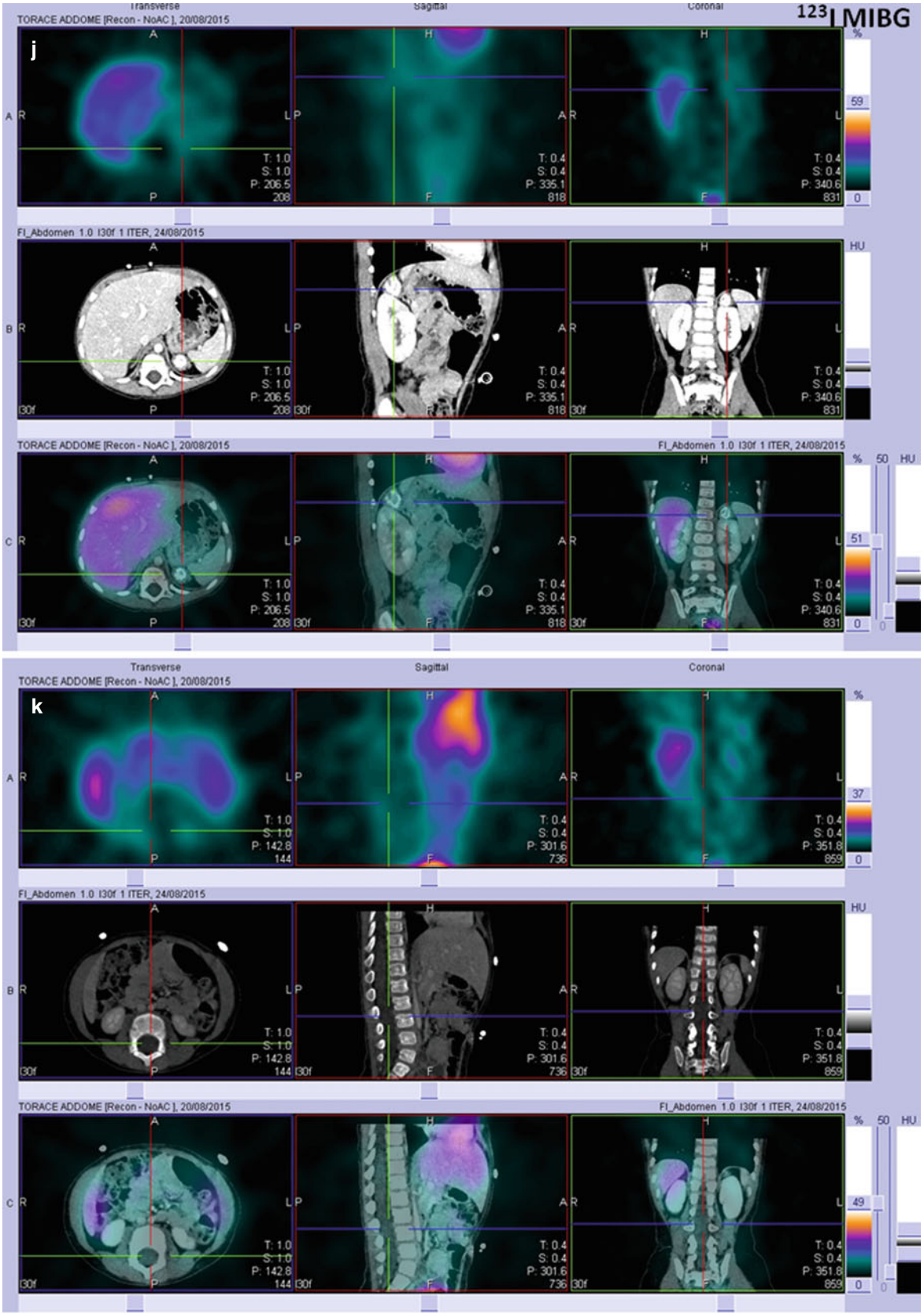

Fig. 13.10 (continued)

13.2.11 Case 13.11 Stage IV Neuroblastoma: Scintigraphic Evidence of Persistent Disease

A 15-month-old baby refers to our emergency for left orbital swelling and exophthalmos; suspecting a periorbital cellulitis, a brain CT scan is performed, which shows a pathological tissue starting from left temporofrontosphenoidal region and infiltrating the left wing of sphenoid bone and lateral wall of the orbit (Fig. 13.11a–d). To complete the study, a whole-body CT (Fig. 13.11e, f) is performed, and a neoplasia in the left adrenal gland is identified. For the characterization of the neoplasia, a biopsy of the adrenal mass is performed, and the suspected diagnosis of neuroblastoma is confirmed. Consequently, a MIBG scintigraphy is scheduled for staging and shows radiotracer uptake in the mass and bone and bone marrow involvement (in particular, in skull base) (Fig. 13.11g). Genomic profile shows NMYC amplification.

Patient is treated according to NBHR European protocol – N7 arm

At the end of the induction treatment, a new balance of disease by CT scan, bone and bone marrow biopsy, and MIBG scan is performed. CT scan shows a partial response of primary tumor and stable disease in the left orbit. One of two bone marrow biopsies was positive for infiltration of disease; MIBG scintigraphy shows persistence of disease compared with the staging (Fig. 13.11h). For this reason, patient receives TVD (topotecan-vincristine-doxorubicin) intensification chemotherapy regimen according to the protocol NBHR01.

Then, the girl undergoes surgery on primary tumor and further chemotherapeutic treatment.

At last follow-up, MIBG scintigraphy shows persistence of disease in skull and orbits, with no other areas of metastatic involvement (Fig. 13.11i, j.)

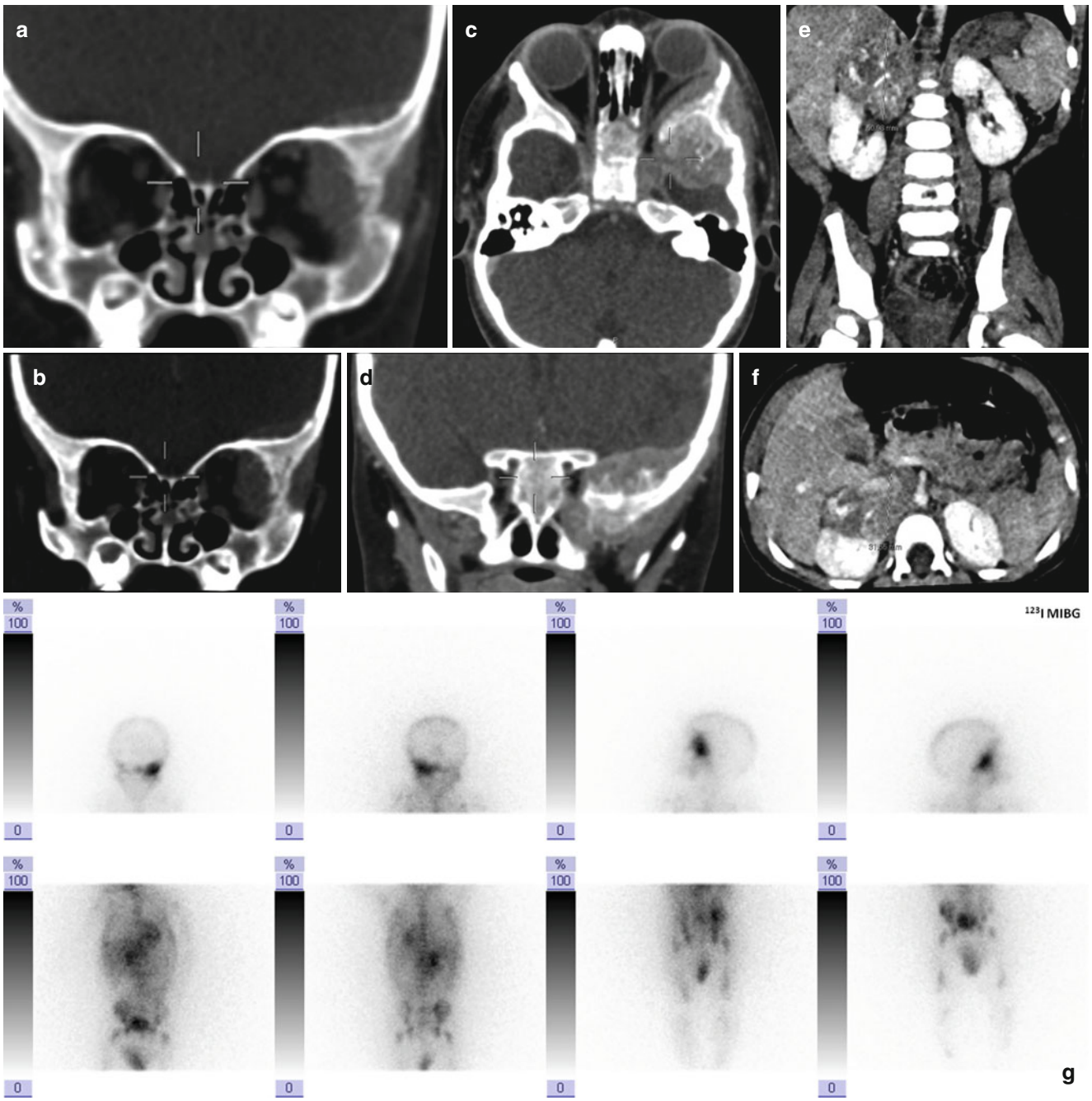

Fig. 13.11 (**a**–**f**) Contrast-enhanced CT: MPR coronal image of the head shows a large lesion originating in the bone marrow, as evidenced by bone destruction on bone windows (**a**, **b**), and then extending to paraosseous soft tissues, causing intraorbital or extratransverse intracranial soft tissue masses with an inhomogeneous enhancement after contrast media administration, better seen on soft tissue windows (transverse and MPR coronal images. (**c**, **d**) Abdomen CT scan shows a large, infiltrating neuroblastoma arising from right adrenal gland, appearing nonhomogeneous after contrast agent administration (MPR coronal and transverse images (**e**, **f**), with large, amorphous calcifications in the contest. The lesion completely encases right renal vessels; the "contact" between the tumor and the aorta and the inferior cava vein is wide. The margins between the tumor and the kidney are ill defined as well as the one between the mass and the liver. Multiple enlarged and nonhomogeneous retroperitoneal node metastases are also evident. (**g**) Staging MIBG scintigraphy (static views) shows nonhomogeneous radiotracer uptake in the abdomen, corresponding to tumor evident on CT. Multiple areas of uptake are evident in skull, skull base, both orbits, sternum, left scapula, ribs, both humeri, both radii, pelvis, femurs, and tibiae, and diffuse uptake in the spine, indicating bone and bone marrow involvement. (**h**) MIBG scintigraphy after treatment (static views): radiotracer uptake still evident shows the tumor in right adrenal lodge (evident on CT scan) and in quite all the sites evident in staging scan, even if intensity of uptake is mildly reduced. This pattern indicates a persistence of disease despite the chemotherapy. (**i**, **j**) MIBG scintigraphy during follow-up (static views, **i**) shows persistent radiotracer uptake in the skull, skull base, and in both orbits, better defined in SPECT-CT fused images (**j**). N other areas of pathological uptake are evident

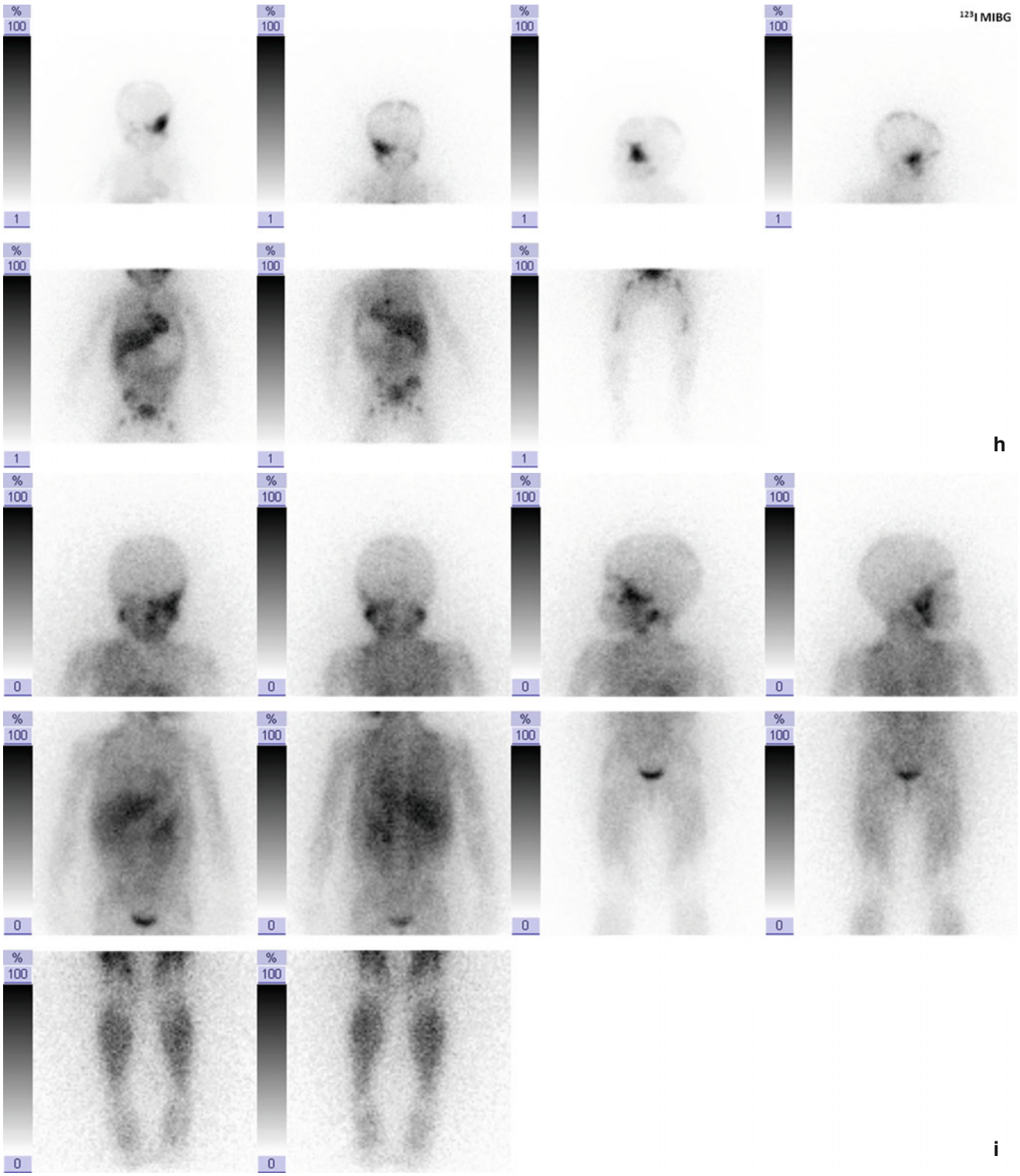

Fig. 13.11 (continued)

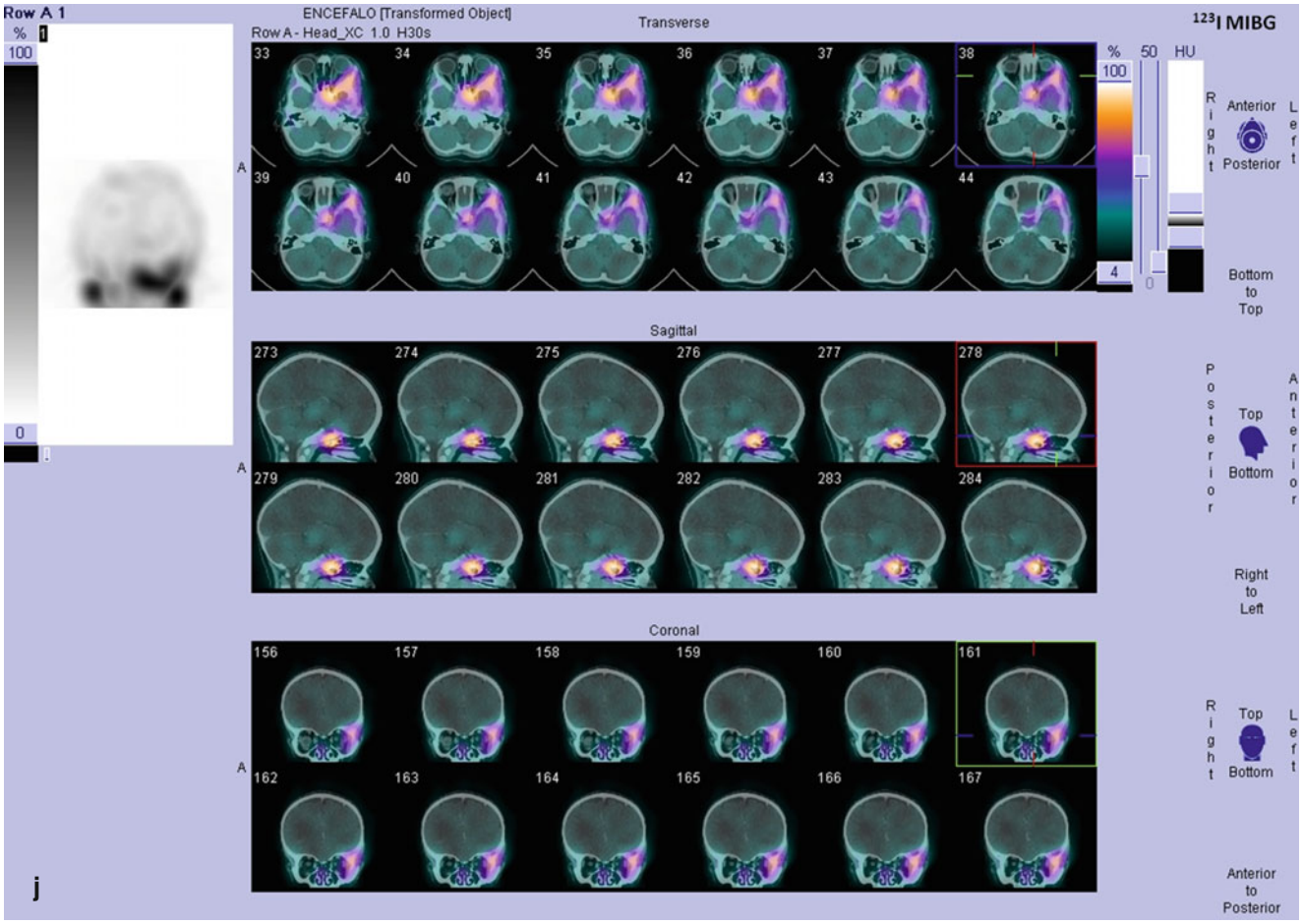

Fig. 13.11 (continued)

13.2.12 Case 13.12: Stage IV Neuroblastoma: Scintigraphic Evidence of Relapse

A 3-year-old child refers to our institution for fever and hard swelling in abdomen at clinical evaluation. Ultrasonography shows evidence of an abdominal mass; a CT detects a large abdominal mass with pleural metastases (Fig. 13.12a–d). MIBG scintigraphy is performed which shows nonhomogeneous radiotracer uptake in the mass and metastases in pleura, and in bone and bone marrow (Fig. 13.12e–g).

Therefore, the girl undergoes chemotherapy, surgery, and radiotherapy; MIBG scintigraphy at the end of treatment shows absence of areas of pathological radiotracer uptake (Fig. 13.12h, i).

During follow-up, a relapse is suspected for increase of LDH value, and a CT scan is scheduled. CT detects a large mass extending above and below the diaphragm, in pre- and paravertebral regions on the midline and on the right paramedian line (Fig. 13.12j–m), and then the girl undergoes a MIBG scintigraphy to restage the disease. The scan shows intense radiotracer uptake in the mass, without other areas of pathological uptake (Fig. 13.12n, o)

Currently, the girl is following chemotherapeutic treatment.

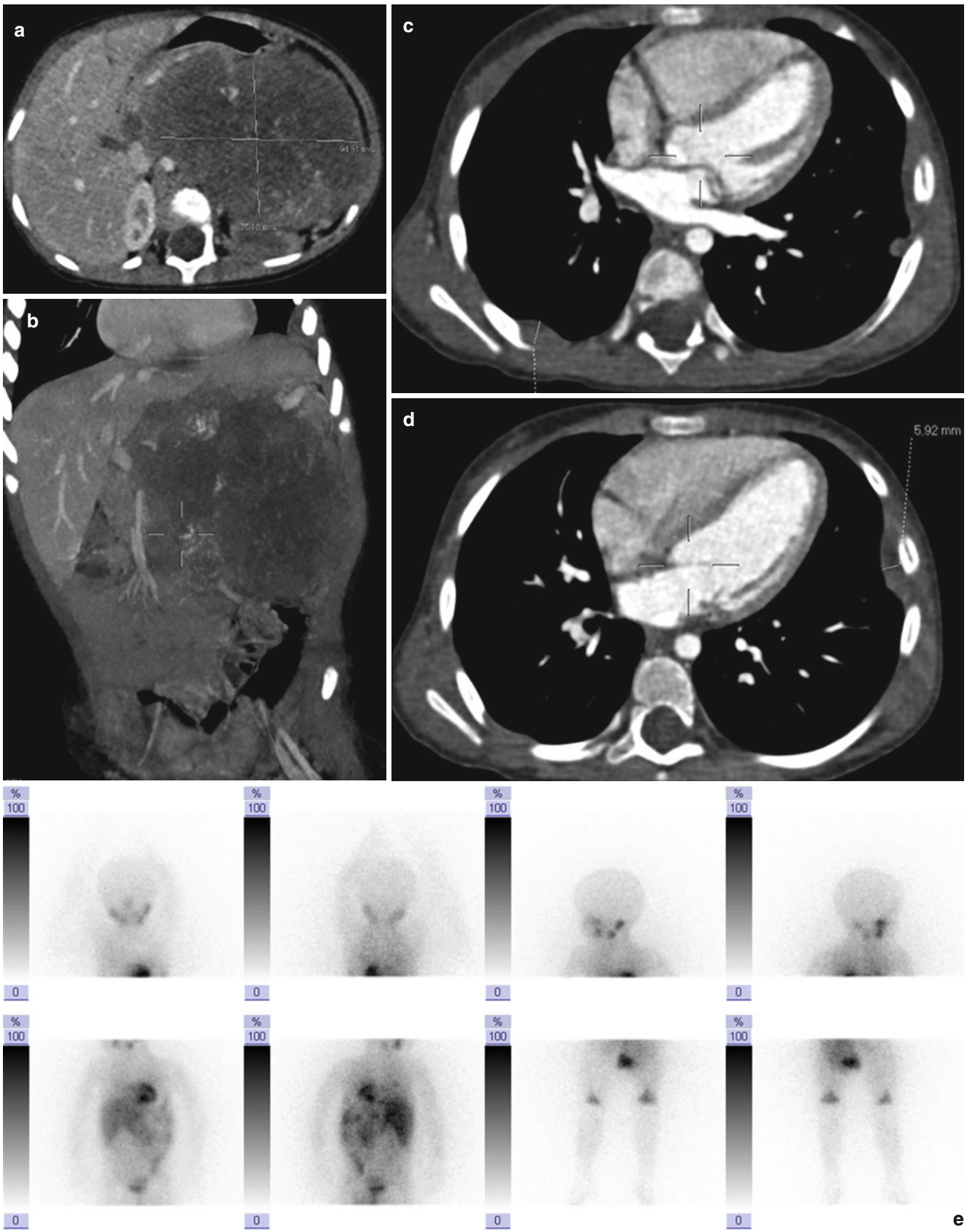
a
b
c
d
5.92 mm
%
100
0
e

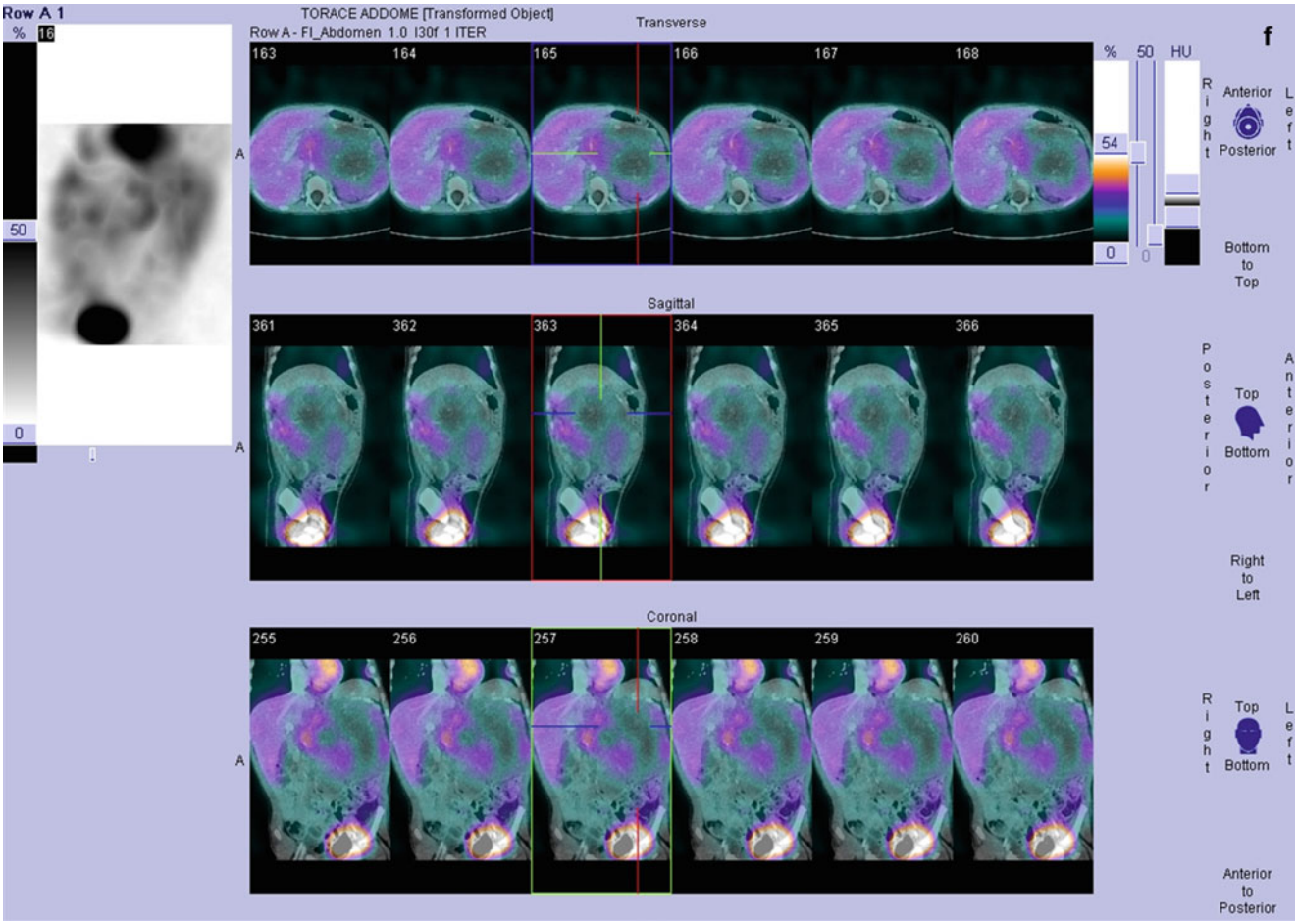

Fig. 13.12 (continued)

Fig. 13.12 (**a**–**d**) Contrast-enhanced CT: left adrenal infiltrating mass with wide retroperitoneal spread (MPR coronal and transverse images, **a**, **b**) and pleural metastases (transverse images, **c**, **d**). (**e**–**g**) MIBG scintigraphy (static views, **e**) shows nonhomogeneous radiotracer uptake in the large mass evident on CT, located in left abdomen, and crossing the midline; it presents wide hypoactive areas, as for colliquative necrosis (often seen in NB). Focal areas of intense radiotracer uptake are evident in distal femurs. SPECT-CT fused images confirm nonhomogeneous radiotracer uptake in the mass (**f**) and show uptake in the pleural lesions evident on CT (**g**). (**h**, **i**) MIBG scintigraphy after treatment (static views, **h**): no evidence of areas of pathological radiotracer uptake; SPECT images confirm this finding (**i**). (**j**–**m**) Contrast-enhanced CT. MPR coronal (**j**), sagittal (**k**), and transverse (**l**, **m**) images show a large mass extending above and below the diaphragm, in pre- and paravertebral region on the midline and on right paramedian line. The lesion is not homogeneous, hypodense after contrast agent administration, without inner calcified areas. It is oval-shaped with ill-defined borders and is about 58 × 55 × 53 mm in size. (**n**, **o**) Restaging MIBG scintigraphy shows intense radiotracer uptake in upper abdomen, above and below the diaphragm, in paravertebral region, corresponding to the mass evident on CT. No other areas of pathological uptake of radiotracer are present. In this case, SPECT-CT fused images (**o**) are mandatory for accurate evaluations of the lesion and its metabolic pattern

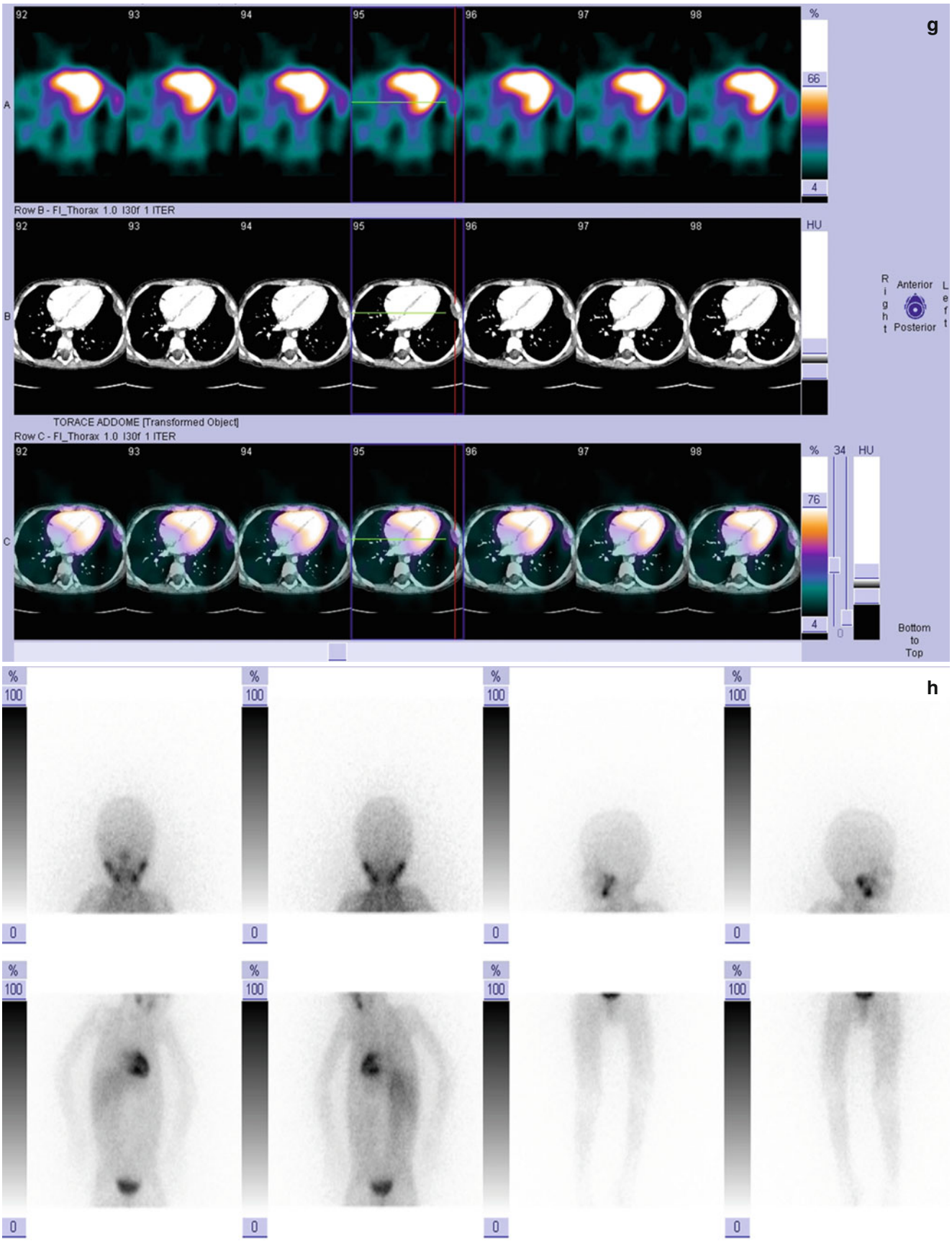

Fig. 13.12 (continued)

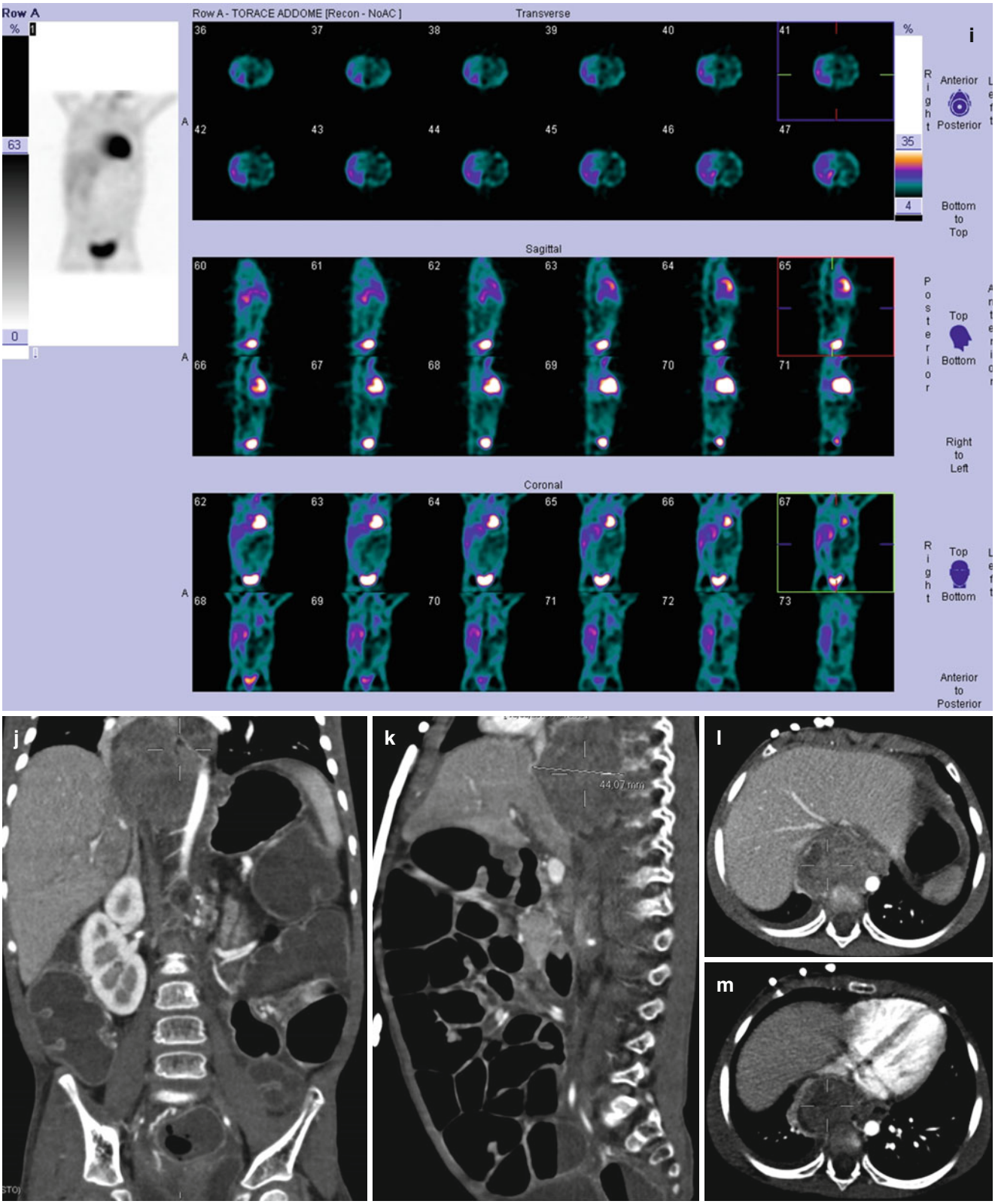

Fig. 13.12 (continued)

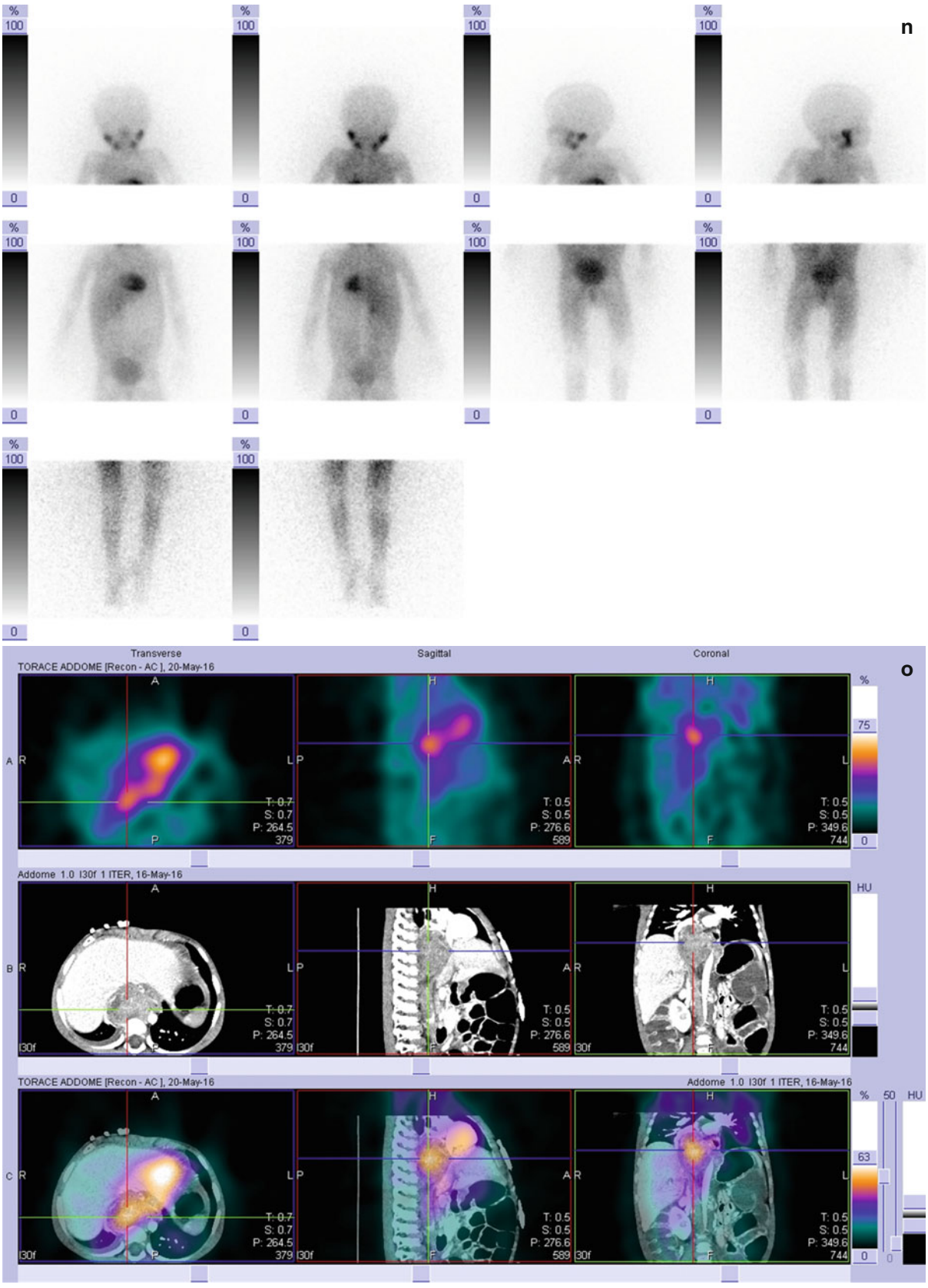

Fig. 13.12 (continued)

13.2.13 Case 13.13 123I-MIBG Scintigraphy in the Evaluation of Patients Eligible for 131-MIBG Therapy

A 13-year-old girl affected by relapsed NB. She had surgery at 5 years of age for an abdominal paravertebral NB Stage I with unfavorable histology, NMYC-negative and multiple further therapy for local recurrence. After 2 years of wellness, the girl experienced an ascend relapse of disease localized in the pleura.

In Fig. 13.13 are displayed restaged 123I-MIBG scintigraphy (a-b) and CT scan (Fig. 13.13c–g). The girl was treated with a course of chemotherapy, and the evaluation of disease at the end of treatment showed stable disease. For this reason, a radiometabolic therapy with I131- MIBG was scheduled (Fig. 13.13l, m), and she received 15 mcg/kg + Melphalan followed by PB stem cells rescue, before therapy.

Although there was a good clinical response to therapy with wellness, at last follow-up, the girl experienced a relapse in lung.

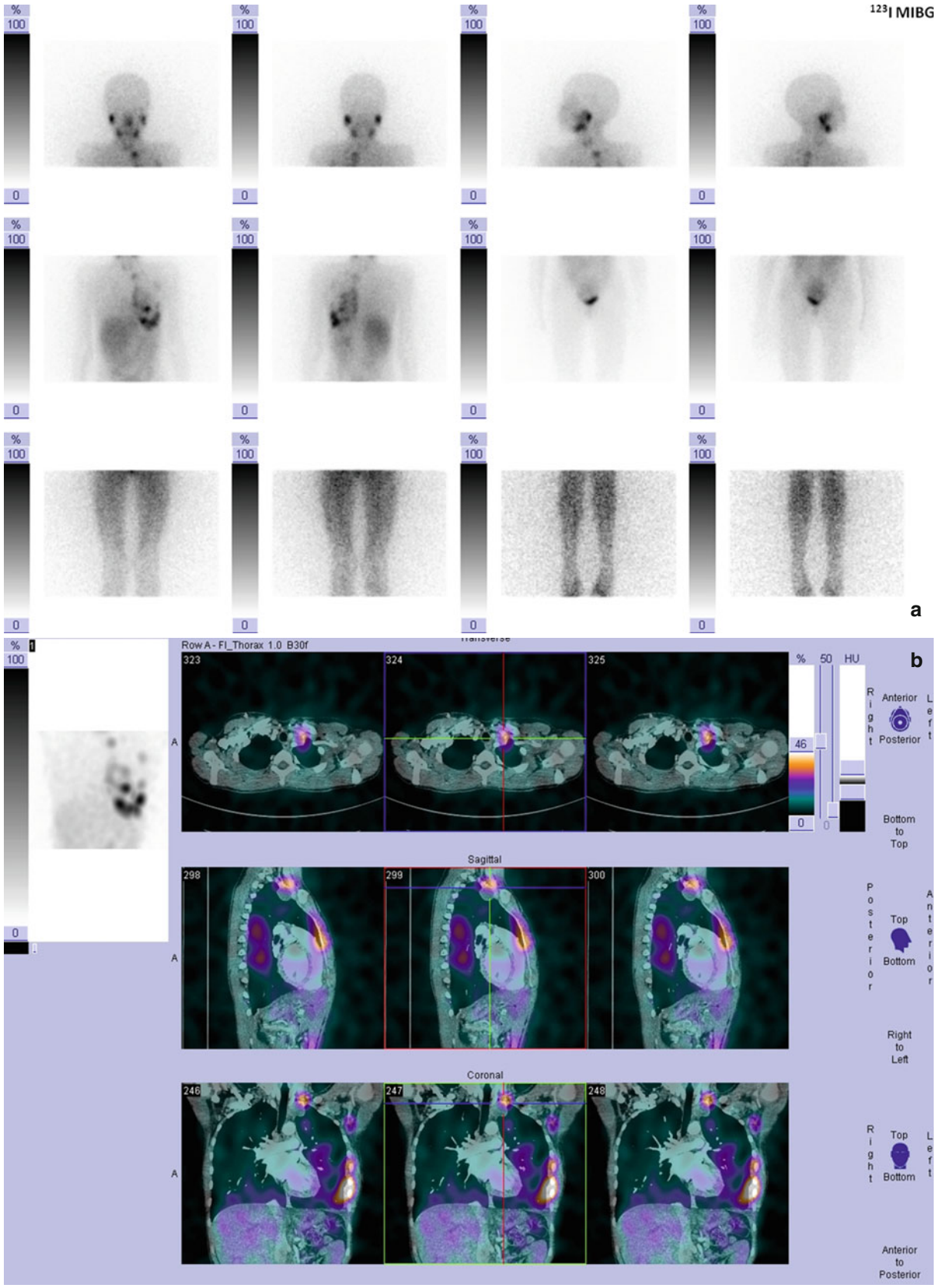
123I MIBG
a
b
Row A - FI_Thorax 1.0 B30f
323
324
325
Anterior
Posterior
Right
Left
Bottom to Top
Sagittal
298
299
300
Top
Bottom
Posterior
Anterior
Right to Left
Coronal
246
247
248
Top
Bottom
Right
Left
Anterior to Posterior

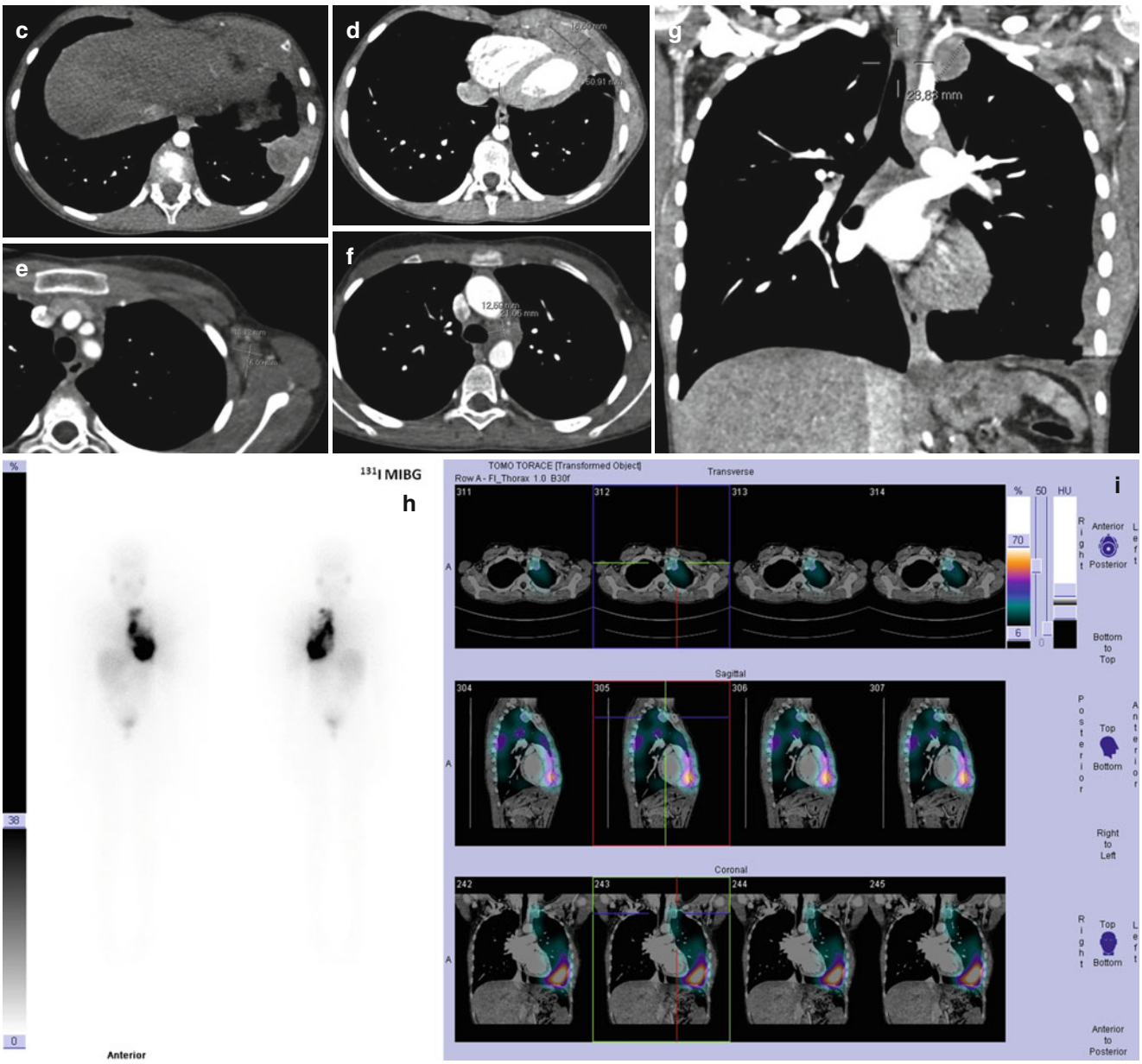

Fig. 13.13 (continued)

Fig. 13.13 (**a**, **b**) 123I-MIBG scintigraphy (static views, **a**) shows multiple focal areas of intense uptake in left hemithorax; SPECT-CT fused images (**b**) localize these areas in correspondence of nodular lesions detected by CT scan in upper left mediastinum and in quite all parietal pleural membranes of left hemithorax; radiotracer uptake is also evident in a tissue in cardiophrenic angle. MIBG uptake is also evident in a pathological tissue in left axilla. (**c**–**g**) Contrast-enhanced CT shows multiple solid and nonhomogeneous nodules located in the superior mediastinum (MPR coronal image, **g**), at the left pulmonary hilum and along the chest wall in subpleural region (transverse image, **c**); the presence of a soft tissue mass in the middle mediastinum, in the aortopulmonary window (transverse image, **f**), and in the left axilla fatty space (transverse image, **e**), respectively, is also observed. (**i**–**h**) 131I-MIBG scintigraphy after administration of therapeutic activity (whole-body, **h**, and SPECT-CT fused images, **i**) confirms the finding of diagnostic 123I-MIBG scintigraphy

Bibliography

1. Giammarile F, Chiti A, et al.; EANM. EANM procedure guidelines for 131I-meta-iodobenzylguanidine (131I-mIBG) therapy. Eur J Nucl Med Mol Imaging. 2008;35(5):1039–47.
2. Monclair T, Brodeur GM, Ambros PF, Brisse HJ, Cecchetto G, Holmes K, Kaneko M, London WB, Matthay KK, Nuchtern JG, von Schweinitz D, Simon T, Cohn SL, Pearson AD, INRG Task Force. The International Neuroblastoma Risk Group (INRG) staging system: an INRG Task Force report. J Clin Oncol. 2009;27(2): 298–303.
3. Olivier P, Colarinha P, et al. Guidelines for radioiodinated MIBG scintigraphy in children. Eur J Nucl Med Mol Imaging. 2003;30(5): B45–50. Epub 2003 Mar 26.